ELSEVIER

Contents lists available at ScienceDirect

# Additive Manufacturing

journal homepage: www.elsevier.com/locate/addma



#### Review

# Recent advances in ink-based additive manufacturing for porous structures



Zipeng Guo, Chi Zhou

Department of Industrial and Systems Engineering, University at Buffalo, The State University of New York, Buffalo, NY 14260, USA

#### ARTICLE INFO

# Keywords: Additive manufacturing 3D printable ink Multi-scale porous structure Multi-functionality

#### ABSTRACT

The use of porous structures is an ancient wisdom, people found its importance ever since we began to understand nature. The evolution of porous structure gives rise to multi-scale (combined nano-, micro-, and macro-) porous networks. Traditional manufacturing technologies have challenges in creating shape-complex and conformable porous structures for real-world applications. Additive manufacturing (AM) with the capability of assembling various materials with complex and customized architectures is rapidly developing. With the advancement of material development, the integration of AM and porous structure offers unparalleled and emerging opportunities for concept-to-design-to-fabrication of multi-scale porous networks, enabling the multi-functionalities of the 3D printed specimen and broadening its applications. Herein, we provide a comprehensive review of the state-of-the-art ink-based AM techniques for 3D printing porous structures. The ink design principle, ink composition, and printability are thoroughly discussed. The methodologies of various AM technologies for porous structures are analyzed. Readers can find a clear experimental guidance toward 3D printing multi-scale porous structures. The synergistic and collective merits of additive manufacturing and porous structure are highlighted and systematically discussed in this review. The challenges and promises of this field for future research are also outlined.

#### 1. Introduction

A porous structure is typically defined as a solid matrix with a considerably large void fraction inside a distinct shell. The pores appear as spatial confiement of air, with the individual pore size ranging from nanometric to macroscale. As opposed to a solid structure, the porous structure integrates large surface area, light weight, and high adsorption capacity. Such unique property predestines the porous structure for enormous applications, including thermal insulation [1], electrochemical energy storage [2], tissue engineering [3], contaminant removal [4], water treatment [5], and catalyst [6]. These emerging applications tackle real-world challenges, such as renewable energy, green energy [6], sustainable manufacturing [7], environmental protection [8], bone grafting, and tissue transplantation [9]. The valuable applications, in turn, continuously drive the evolution of modern engineering science and technology.

The conventional in-situ foaming method is widely used for producing porous products, such as sponges, polymeric foams for packaging, and even foods (bread and cakes) [10]. The sacrificial templating and replica templating methods are also used to produce insulation pads, filtration foam [11], etc. The sol-gel method coupled with the

subsequent solvent exchanging process is efficient for creating porous ceramic structures [12]. Molding is the most widely used manufacturing method for shaping the porous structure in simple bulk geometry. However, with the rapid development of nanomaterials for porous structure, customized and conformable shape is highly intended. Moreover, accurate porosity control and spital arrangement of pores play a vital role in realizing certain functionalities. These new challenges are far exceeding the capability of traditional design and manufacturing technologies, hindering the fabrication of multi-scale and multi-functional porous networks in three-dimensional (3D) objects.

Additive manufacturing (AM), also known as 3D printing, is a generic and efficient process for building custom-designed complex 3D objects in a bottom-up fashion. Based on the designed digital model, AM technologies can directly fabricate the model with various materials. As the name implies, AM continuously adds the building blocks to fabricate an object. In contrast, the traditional manufacturing (subtractive manufacturing) methods remove material by milling, turning, drilling, cutting, or other means. AM encompasses a set of technologies that are rapidly developed in recent years, such as Direct Ink Writing (DIW), Stereolithography (SLA), Inkjet Printing (IJP), Fused Deposition Modeling (FDM), Selective Laser Sintering (SLS), Binder Jetting (BJ),

E-mail address: chizhou@buffalo.edu (C. Zhou).

<sup>\*</sup> Corresponding author.

and Electron Beam Melting (EBM). These technology innovations give rise to the versatile assembly of various materials into 3D objects with high resolution, high shape fidelity, and high complexity.

With all the fascinating properties of the porous structure and additive manufacturing technologies, researchers are investing massive efforts in combining them to take advantage of AM technologies for 3D printing porous structures. Despite tremendous progress and advancement made in the past decades, two major challenges exist in this research field:

- I. The foremost challenge is the limitation of fabricating submicronscale and nano-scale porous features by the AM technologies alone. As shown in Figs. 1 and 2, most AM approaches can reach the resolution for printing the macro-scale porous structures. Despite the fact that the resolution of the common AM technologies has been continuously improved in recent years, a bottleneck appears at the process resolution which can hardly be beyond the sub-micron scale. In particular, both the lateral resolution and vertical resolution are limited by the nature of digitalized manufacturing process of AM. To overcome the resolution constraint, researchers seamlessly merged the AM technologies to the conventional porous material manufacturing processes, developing an integrated and interdisciplinary strategy for 3D printing of porous structures. The feedstock materials are firstly 3D printed using the AM technologies, followed by the traditional templating or solvent exchanging methods to create the micro-scale and nano-scale porous networks. Such combination also rises to the 3D fabrication of multi-scale porous structure that allows for regulating the pore size, pore shape, and pore arrangement and morphology. Furthermore, the multi-scale network was prohibitively challenging to achieve by the conventional manufacturing methods alone.
- II. The other challenge is that most building block materials are not compatible with direct assembly by AM technologies. Some intrinsic porous materials such as ceramic aerogels in solid-state cannot be directly handled or assembled by existing AM approaches. On the other hand, most of the precursor in fluid-state is also not compatible with 3D printing, due to its high fluidity preventing the printed ink



**Fig. 1.** An overview of ink-based additive manufacturing technologies for porous structures and their applications.

from standing freely in 3D space. Therefore, preparing printable stock materials with suitable rheological properties is vital in AM processes, including inkjet printing, extrusion-based direct ink writing, and stereolithographic printing. To this end, we defined the ink-based additive manufacturing as the process of utilizing fluid inks, which contain building block materials, solvents, and additives, with compatible AM techniques to build 3D objects in a layer-by-layer fashion.

The 3D printed multi-scale porous structure readily offers multifunctionalities that can be developed for broad applications. The structure-property-performance is always the guideline to the design of structure, material, and process. Therefore, in this review article, we present a panoramic view of this fast-developing area, and most importantly, analyzed the state-of-the-art methodologies. Briefly, we first review the ink design principle for printing the porous structure, discuss the ink composition, and analyze the printability of different types of ink. Next, the ink-based additive manufacturing processes were summarized and evaluated in Section 3. In particular, we highlight the significance of combining additive manufacturing and traditional manufacturing to produce multi-scale porous networks. For the third part of the review, we present the post-processing process for AM, which depicts the combination of traditional manufacturing and AM process. Readers can find a clear experimental guidance toward 3D printing of multi-scale porous structures throughout the first three sections. Then, we highlight the applications of the 3D printed porous structures, and how it tackles real-world challenges. In the last, we provide a perspective of this field, along with the challenges and opportunities for future development. We hope this review can help the communities from academia and industry to understand the recent advances and challenges in this multidisciplinary field.

#### 2. Ink design principle and preparation

#### 2.1. Ink category

Depending on the target pore size and the compatibility with 3D printing techniques, we categorize the ink into three types, namely Newtonian ink, non-Newtonian ink, and photosensitive ink. The Newtonian ink possesses low viscosity, and it's suitable for the droplet-based inkjet 3D printing. The inkjet printing is capable of assembling 1D [13-16], 2D [17-20], and 3D [21-23] materials into the pre-defined large-scale geometries. The composition is relatively simple, mainly consisting of material feedstock and solvent, binder is also added to the ink for maintaining integrity after printing [24,25]. A non-Newtonian fluid is also referred to as colloidal ink, in general it has a higher viscosity than the Newtonian fluids, and its viscosity is dependent on the shear rate. When the shear rate increases, the ink viscosity quickly decreases, and becomes "thinner" under shear. Therefore, a shear-thinning non-Newtonian ink is suitable for the filament-based direct ink writing (DIW) process [26,27]. Similar to the Newtonian ink, the composition of colloidal ink consists of the material feedstock, solvent, and additives for tuning the rheological behavior. The colloidal ink has a much higher volume fraction of material feedstock compared to the Newtonian ink, thus it can produce a higher yield. A high mass loading of material can promote the enhanced performance after printing [28]. The photosensitive ink is designed for the stereolithography (SLA) method. To facilitate the photo-crosslinking process, the photocurable component is essential in the ink. The ink solidifies through the light-induced curing, thereby forming the designed 3D geometries. The post-processing is required to remove the photocurable component in the fabricated sample, and eventually form the porous structure.

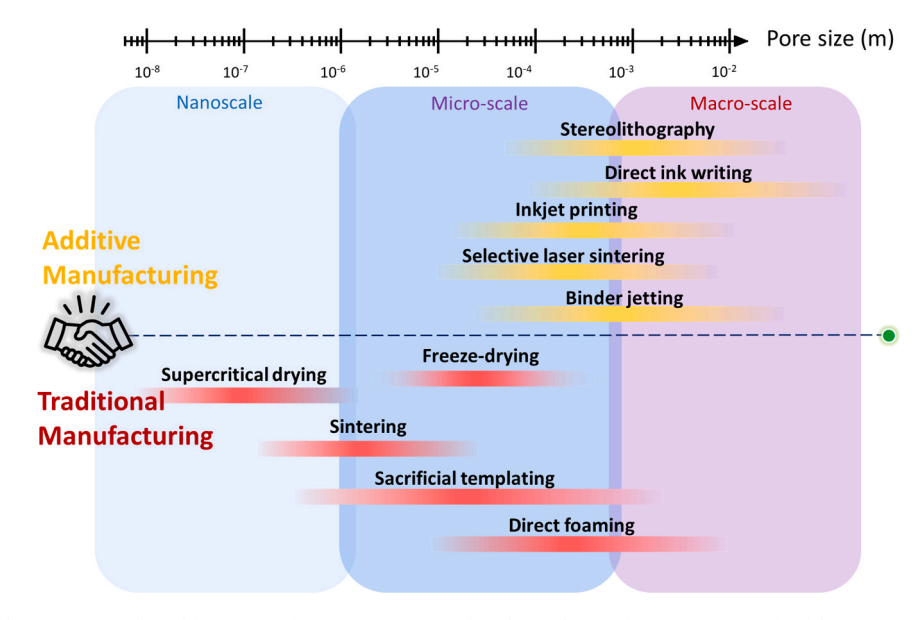


Fig. 2. The complementarity of the additive manufacturing process and traditional manufacturing process for fabricating 3D porous structures.

#### 2.2. Ink pre-processing for the porous structure

#### 2.2.1. Newtonian ink

The mainstream Newtonian ink is the particle suspensions, where the metal oxide, ceramic, or carbon-based particles are dispersed into the solvent. In most cases, the particles are suspended rather than dissolved in the solvent to form a colloidal ink. Therefore, after printing and removing the solvent, the samples retain the property and performance of the original feedstock particles. Table 1 shows a summary of the research works where Newtonian ink was used for additive manufacturing. By combining the inkjet printing with the pre-defined solvent removal process, a porous network can be derived from the space previously occupied by the solvent. This route requires the post-processing either by solvent sublimation at freezing point [18,29,30] or solvent removal at the supercritical point [31]. The water-based ink is favorable for the freeze-drying process, where water can be frozen either in-situ during the printing process or frozen in the liquid nitrogen

environment during the post process. Though effective, the yield from the particle suspension ink is limited. To overcome this challenge, some research works utilize the phase-changing ink, where the phase change is initiated chemically or thermally [32–37]. Materials like gallium (melting point at 30 °C), paraffin wax (melting point at 50 °C), DMSO (Dimethyl Sulfoxide, melting point at 19 °C) and water (melting point at 0 °C) are good candidates for the thermally initiated phase-change ink. The chemically initiated phase-change ink mainly includes the photo-curable component, and the solidification is enabled by the photo-crosslinking [38–41].

#### 2.2.2. Non-Newtonian ink

With the facile accessibility, preparation and processing, Non-Newtonian fluids are the most widely used ink in this field. In conjunction with the direct ink writing process, higher loading of the material feedstock can be realized using this type of ink. Furthermore, multiscale and multifunctional structures and devices can be assembled

**Table 1**Summary of Newtonian ink used in AM process for porous structures.

Feedstock material	Feedstock dimension	Solvent	3D printing technique	Pore generation approach	Post-processing method	Ref.
Silver nanowire	1D	Isopropyl alcohol (IPA) and ethylene glycol	Inkjet	Solvent exchange	Ambient pressure drying and heat treatment	[13]
		Isopropyl alcohol (IPA)	Inkjet	Solvent exchange	Vacuum drying	[14]
liquid phase Bismuth telluride nanowire	1D	Deionized water	Inkjet	Solvent exchange	Ambient pressure drying and heat treatment	[15]
Graphene oxide	2D	Deionized water	Inkjet	Freeze-casting and solvent exchange	Freeze-drying	[18]
Graphene oxide and ammonium thiomolybdate	2D	Deionized water	Inkjet	Solvent exchange	Freeze-drying	[17]
PEDOT:PSS	2D	Isopropanol, Butanol and pentanol	Inkjet	Solvent exchange	Ambient pressure drying and heat treatment	[19]
Silver nanowire	2D	Acetone and 2-propanol	Inkjet	Solvent exchange	Ambient pressure drying	[20]
Silver nanoparticle, copper, cobalt	2D	Methanol, n-tetradecane and 1,2- Dichlorobenzene	Inkjet	Solvent exchange	Ambient pressure drying	[22]
Alumina	3D	Deionized water	Inkjet	Solvent exchange	Ambient pressure drying and heat treatment	[21]
Alumina	3D	Paraffin wax	Inkjet	Solvent exchange	Ambient pressure drying and heat treatment	[34]
Titania	3D	Deionized water	Inkjet	Solvent exchange	Ambient pressure drying and heat treatment	[23]
Titania, silver nitrate	3D	Poly(ethyleneoxide), Polyethylene glycol, Deionized water	Inkjet with laser irradiation	Solvent exchange	Ambient pressure drying	[41]
Cadmium selenide	3D	Methanol, toluene, n-hexane, potassium hydroxide	Inkjet	Solvent exchange	Supercritical drying	[31]

by 3D printing of colloidal ink. Matter et al. illustrate the design principle of a non-Newtonian ink [12]. Two aspects are of great significance for preparing the printable colloidal ink, including the homogenous dispersion of solid particles and the stability of ink against aggregation and sedimentation. In particular, the small (sub-micron sized) spherical particles are favorable for dispersing the feedstock into the solvent. The rate of the diffusion could rapidly increase with the decreasing particle radius, and the sedimentation caused by the gravitational forces is less for smaller particles. Ball milling is often used for modifying the size and shape of the raw material [42-45]. The Brownian motion depicts the random motion of particles dispersed in the solvent. Solvent with a higher temperature has a higher level of thermal equilibrium, thereby allowing for easier and more uniform dispersion of the particles. The mixing step often requires prolonged time (in hours) to ensure homogeneity. Using a high vacuum (less than 0.5 atm) and high speed (more than 1500 rpm) mixing method can overcome this obstacle [46,47].

When selecting or synthesizing the solid material feedstocks for preparing non-Newtonian ink, it is preferable to use the one with high solubility to reach a high ink loading. Surface modification (adding amino or hydroxyl groups) is a straightforward way to achieve a high solubility in the solvent. Besides, materials in different crystalline phases can have different solubility. For example, the Tricalcium phosphate (TCP) is a porous material that is favorable for biomedical applications. The  $\alpha$ -phase TCP is more soluble than the  $\beta$ -phase TCP, in that  $\alpha$ -TCP is more thermodynamically unstable. Thus, it makes the  $\alpha$ -TCP a better candidate for preparing the non-Newtonian ink.

A stable ink ensures the subsequent continuous ink extrusion and thus guarantees the controllability of the 3D printed shape. The particles within the ink are subjected to the van der Waals attraction, electrostatic repulsion, magnetic interactions, and ligand interactions, these interparticular forces are of importance to the ink stability [48-51]. The feedstock particles tend to be agglomerated when the van der Waals attraction dominates the electrostatic repulsion (DLVO theory) [52,53]. Two routes are typically used to prevent the agglomeration in the ink preparation: (1) introduce the extra electrostatic repulsion to overcome the van der Waals interaction; (2) increase the steric repulsion to reach an equilibrium between the interactions. The dispersing agent is widely used as an additive to keep the ink uniform and homogenous. Typical dispersing agent, or dispersant has dissociable functional groups like hydroxyl (OH), carboxyl (COOH), amino (NH), amino (HN2), ammonium (NH<sub>4</sub><sup>+</sup>), and sulfonate (SO<sub>3</sub><sup>-</sup>). Once the dispersant is mixed with the ink, these functional groups promote extra steric repulsion between the particle, which subsequently neutralizes the van der Waals attractions and stabilizes the ink. The dispersant component could be removed by the subsequent heat treatment. The surfactant chemicals such as benzethonium chloride (BZT), sodium dodecyl sulfate (SDS), and cetrimonium bromide (CTAB) can introduce the surface potential and further develop electrostatic repulsion in ink [7,54]. The ink stability can be obtained with a sufficiently large repulsive force that exceeds the van der Waals attraction.

The pre-processing of the non-Newtonian ink for the printed porous structure is a critical step, and it determines the final pore size, pore distribution and pore density. The conventional drying method (freezedrying and supercritical drying) can be combined with the direct ink writing to create the stochastic porous network. Zhao et al. seamlessly adopt the conventional sol-gel process to produce the silica aerogel into the direct ink writing approach [55]. The silica sol was prepared as non-Newtonian ink for the DIW, the 3D printed structure was gelled by Ammonia vapor-based pH change, and eventually dried from supercritical CO2. Towards a better control of the pore shape, the oil-water emulsion method and the direct foaming method have been adopted with DIW [56]. The oil-phase solvent was added to the colloidal ink in a dropwise fashion, the oily and spherical drop can be maintained within the ink, the mixture was then printed with DIW [57]. Similarly, the emulsion can be produced by adding sunflower oil [58], corn oil [59], Dichloromethane (CH<sub>2</sub>Cl<sub>2</sub>) [60], and n-Octane [61]. The oil-water

mixture requires vigorous blending to convert the coarse emulsion into fine drops, typically by the rotary mixer (centrifugal mixer) [58], sonicator [60], and high-pressure homogenizer [62].

The direct foaming is one of the most cost-effective and scalable methods for creating porous structures. Muth et al. [63] developed the foamed ink by vigorously stirring. To achieve a more stable gas-liquid interface, Guo et al. [7,64] used the surfactant-like foaming agent to create the gaseous bubble within the ink. The surfactant-like foaming agent creates the electrostatic repulsion at the gas-liquid interface, thus ensuring the gas bubbles' stability. The porosity of the printed sample can be controlled and tailored by the concentration of the foaming agent. Towards a multi-scale hierarchical structure with precise control over the pore shape and size, the sacrificial templating combined with DIW can produce such structure. The sacrificial beads were added to the colloidal ink, then the beads were subsequently removed by the heat treatment. Huang et al. [65] utilized the Polymethyl methacrylate (PMMA) microsphere [66] in different sizes (from 0.5  $\mu m$  to 50  $\mu m$ ) as the sacrificial beads. By high-speed mixing (2000 rpm), the PMMA microsphere can be uniformly blended with the ink. Jin et al. adopt a similar route by using the yeast cell as the sacrificial material [67]. A combined method of integrating emulsion templating and sacrificial templating was used to create multiple levels of the hierarchical porous

Table 2 summarizes the works where non-Newtonian ink was used for additive manufacturing of porous structures. In most cases, a rheological modifier component is necessary in the ink. The ink can be tuned to present the shear-thinning behavior by adding the rheological modifier, thus ensuring favorable ink printability. This type of chemical usually has a high molecular weight. For example, the cellulose [7,44,63,68–70] is widely used as the rheological modifier, which can be removed by heat treatment. Additionally, owing to the abundant hydroxyl groups on each cellulose molecule, hydrogen bonding can be easily achieved between the cellulose and the material building blocks. Therefore, cellulose also serves as a favorable binder in the ink. A liquid phase rheological modifier such as the Ethanolamine [57], Polyethylenimine [71,72] can play the same role by triggering gelation of the ink

#### 2.2.3. Photosensitive ink

Photosensitive inks are designed primarily for the stereolithography (SLA) 3D printing process. Motivated by the geometrically complexityfree fabrication ability of SLA, the photosensitive ink has been developed for 3D printing porous structures. A typical photosensitive ink is a less viscous Newtonian fluid, which is compatible with a commercially available SLA printer. The photocurable composition includes the monomer and oligomer precursor, photoinitiator and light absorber. Ink with higher-loading particles is more viscous and presents as a non-Newtonian fluid, retrofitting printer becomes necessary to print such viscous inks [79-81]. Table 3 summarizes the works where the photosensitive ink was used. As mentioned in the previous section, a photo-curable component is indispensable in the ink recipe, and it shall be removed by post-processing. The porous structure can be generated by post-processing solvent exchanging at freeze point [82,83], or at supercritical point [84], with the oil-water emulsion template in the ink [62], sugar [85] or salt [86] as the sacrificial template. In certain circumstances, it was found that a macroscopic porous structure printed from the photosensitive ink doesn't preserve the property/performance of the raw building block, or the reproducibility is very limited. The reason can be traced back to the photo-crosslinking process, where the chemical structure of the feedstock material might be broken or degraded by the newly formed polymer network. Such defects could even further deteriorate during the post-processing. To mitigate this shortcoming and maximize the functionality of the printed porous structures, researchers replaced the conventional plain acrylate-based photopolymer resin with the "precursor resin". The precursor resin can not only participate in the photo-crosslinking, but also takes part in a

 Table 2

 Summary of non-Newtonian ink used in AM process for porous structures.

Feedstock material	Solvent	Rheology modifier	Pore generation approach	Post-processing method	Ref.
Silica aerogel	1-Pentanol, hydrogen chloride (HCL)	Poly(propylene glycol) Solvent exchange bis(2-aminopropyl ether)		Supercritical drying	
Graphene oxide (GO)	Deionized water	Fumed silica	Solvent exchange	Supercritical drying	[73]
Graphene oxide (GO)	Deionized water, ammonium carbonate	Fumed silica	Solvent exchange	Supercritical drying	[74]
Graphene oxide (GO), silver nanowires, multi-walled carbon nanotubes	Dimethyl Sulfoxide (DMSO), ethanol	Polyethylene glycol (PEG)	Solvent exchange	Supercritical drying	[37]
Alumina	Camphene	_	Freeze-casting and solvent exchange	Freeze-drying	[75]
Polycaprolactone (PCL)	Glacial acetic acid (GAC)	_	Freeze-casting and solvent exchange	Freeze-drying	[76]
Lithium Iron Phosphate (LiFePO <sub>4</sub> )	NMP (N-methyl-2-pyrrolidone)	Poly vinylidene Fluoride (PVDF)	Freeze-casting and solvent exchange	Freeze-drying	[77]
Silicon oxycarbide	Isopropyl alcohol	Cross-linking agent (GF91)	Sacrificial templating (Template: Polymethyl methacrylate)	Ambient pressure drying and heat	[65]
		(GP 91)	rolymethyl methaciylate)	treatment	
Titanium diisopropoxide bis	Ethanol, deionized water,	Polyvinylpyrro-lidone	Sacrificial templating (Template:	Heat treatment and	[78]
(acetylacetonate) (TIA)	dodecylbenzenesulfonic acid (DBSA), Ammonium hydroxide (NH <sub>4</sub> OH)	(PVP)	Silica nanosphere)	chemical etching	
Silica	Deionized water,	_	Emulsion templating (Template: Oil	Ambient pressure	[59]
	Phosphatidylcholine (PC), hydrogen chloride (HCL)		drops)	drying and heat treatment	
Titania	Deionized water, stearic acid	Ethanolamine	Emulsion templating (Template: Polyoxyethylene sorbitan monostearate (P60) and Lanolin)	Ambient pressure drying and heat treatment	[57]
Alumina	Deionized water, hydrogen chloride (HCL)	poly(acrylic acid), methylcellulose	Emulsion templating (Template: noctane)	Ambient pressure drying and heat treatment	[61]
Hydroxyapatite (HAP, with hydrophobic modification)	Dichloromethane (DCM), deionized water	Silica nanoparticle (partially hydrophobized)	Emulsion templating (Template: water-in-oil)	Ambient pressure drying and heat treatment	[60]
Silica aerogel	Deionized water	Hydroxypropyl methylcellulose (HPMC)	Direct foaming (foaming agent: Cetrimonium bromide and Sodium dodecyl sulfate)	Ambient pressure drying and heat treatment	[7]
Silica (Surface modified with amino group)	Deionized water	Hydroxypropyl methylcellulose (HPMC)	Direct foaming (foaming agent: Cetrimonium bromide)	Ambient pressure drying	[64]
Alumina (partially hydrophobized)	Deionized water, Sodium hydroxide (NaOH)	Hydroxypropyl methylcellulose (HPMC)	Direct foaming (gaseous bubbles)	Ambient pressure drying	[63]

**Table 3**Summary of photosensitive ink used in AM process for porous structures.

Feedstock material	Photosensitive component	Photo-initiator	Pore generation approach	Post-processing method	Ref.
Silica precursor	-	Diphenyl(2,4,6-trimethylbenzoyl)phosphine oxide (TPO)	Solvent exchange	Supercritical drying	[84]
Hydroxyethyl methacrylate (HEMA), Ethylene glycol dimethylacrylate (EGDMA)	Hydroxyethyl methacrylate (HEMA), Ethylene glycol dimethylacrylate (EGDMA)	Phenylbis(2,4,6-trimethylbenzoyl)phosphine oxide (Irgacure 819)	Solvent exchange	Supercritical drying	[91]
Zirconia	Acrylamide, methylenebisacrylamide	2-hydroxy-2-methylpropiophenone	Freeze-casting and solvent exchange	Freeze-drying	[82]
Beta-tricalcium phosphate	Acrylamide, methylenebisacrylamide	2-hydroxy-2-methylpropiophenone	Freeze-casting and solvent exchange	Freeze-drying	[83]
Poly(ethylene glycol) diacrylate (PEGDA), Cellulose nanofibril	Poly(ethylene glycol) diacrylate (PEGDA)	Eosin Y disodium salt (eosin Y), triethanolamine (TEA), 1-vinyl-2 pyrrolidinone (NVP)	Freeze-casting and solvent exchange	Freeze-drying	[92]
Photopolymer	Photosensitive resin (SI500)	-	Sacrificial templating (Template: Sugar)	Washing	[85]
Photopolymer	Poly(ethylene glycol) diacrylate (PEGDA), Clear resin, Spot-E resin	Phenylbis(2,4,6-trimethylbenzoyl)phosphine oxide (Irgacure 819)	Sacrificial templating (Template: Salt)	Washing	[86]
Silver nanoparticle	Dipentaerythritol hexaacrylate (DPHA), trimethylolpropane-triacrylate (TMPTA) and dipropylenglycol diacrylate (DPGDA)	ethyl-4-dimethylaminobenzoate (EDMAB), 2-iso- propylthioxanthone (ITX), 2 benzyl-2 dimethylamoni-1–4-morpholinophenyl- butanone-1 (Irgacure 369), dimethyl-1,2- diphenyllehan-1-one (Irgacure 651), benzophenone	Emulsion templating (Template: Polysorbate 20 and Sorbitan monolaurate)	Vacuum drying and heat treatment	[62]

photo-gelation process, thus the photopolymer network can be coherently combined with the feedstock material [87]. Trimethoxysilylpropyl methacrylate (TMSM) [88] and (3-Aminopropyl) trimethoxysilane (APTMS) [89] have been used as the precursor resin for 3D printing the

porous silica structures. Hu et al. [90] utilized the hydrogel precursor for fabricating the 3D hydrogen-bonded molecular multiferroics. The porous hydrogel network provides an excellent space as a proton reservoir, enabling the modulating of ferroelectric polarization by the

protons. This process creates a versatile bottom-up pathway toward molecular heterogeneous multiferroics design and fabrication. Dong et al. [91] introduced a porogen content (mix of cyclohexanol and 1-decanol) in photosensitive ink, it's miscible with the monomers (HEMA, hydroxyethyl methacrylate) for photo-crosslinking. Upon curing, the porogen content stayed as a secondary phase material in the sample. This route can effectively produce porous structure in nanoscale, owing to the good miscibility in monomer and low viscosity, the solvent-like porogen material can take a large volume fraction in ink (up to 50%). The porogen was subsequently removed during supercritical drying process and thus generated the inherently nanoporous network.

Over the recent years, we have seen the use of commercial photopolymer resin is progressively replaced by customized photosensitive ink for research purposes. Most of the commercial photo-resin can barely bring any functionalities to the final product. Nonetheless, an engineered ink recipe could potentially lead to better performance in the final product.

#### 2.3. Ink printability

#### 2.3.1. Newtonian ink

The accurate and stable droplet jetting behavior is the primary consideration of the Newtonian ink printability. The physical properties of the ink, such as the density, viscosity and surface tension, can have a significant effect on the printability [93,94]. The Ohnesorge number (Oh) is extensively used to characterize the printability, it correlates the ink viscosity  $(\mu)$ , density  $(\rho)$ , and surface tension  $(\sigma)$  with the droplet diameter (L), defined as

$$Oh = \frac{\mu}{\sqrt{\rho \sigma L}} \tag{1}$$

The inverse value of the Ohnesorge number, denoted as Z (Z=1/Oh), defines a printable ink should fall in the range between 1 and 10. When the Z value is less than 1, it indicates the ink is overly viscous, and it forms an unfavorable elongated droplet when jetted out of nozzle. If the Z value is greater than 10, it reveals the viscosity is too less, causing unstable droplet jetting. The satellite droplets may be formed [14,28] with such ink, which compromises the high-resolution drop-on-demand merit of inkjet printing.

Measuring the abovementioned properties of the Newtonian ink poses challenges as the piezoelectric printhead operates in a highfrequency range (in the order of 103 Hz). The characterization instruments, such as a torsional rheometer for the viscosity can hardly reach an equivalent frequency. To overcome this drawback, the customized capillary viscometer has been reported by Wang et al. [95, 96], the core feature utilizes a constant flow generator that produces high shear rates (higher than  $10^4 \, \text{s}^{-1}$ ) and high frequency for operating the viscometer. The alternative method for measuring the printability is the direct imaging method. By using a high-speed charge-coupled device (CCD) camera, the collected droplet patterns were then used for feature extraction and further analysis. Combined with the machine learning (neural network) algorithms, the in-situ closed-loop control can be realized during the printing process [97-99]. An evolution on top of the imaging characterization is developed by Segura et al., where the streaming videos were used for detecting the anomalies, and the real-time control on the printability is achievable with this technique

#### 2.3.2. Non-Newtonian ink

Different from the Newtonian ink, where its viscosity is independent of the applied shear stress, the viscosity of non-Newtonian ink varies with the shear rate. The ink rheological behavior is the major factor to ensure the printability of non-Newtonian ink for the extrusion-based direct ink writing process. At the quiescent state, the ink is expected to exhibit solid-like behavior to maintain the free-standing 3D shape. During the extrusion process, the ink undergoes shear deformation, we

then expect the ink to exhibit fluid-like behavior to ensure a continuous smooth flow, i.e., the ink should be viscoelastic [26]. A typical viscoelastic ink for DIW is the highly viscous and shear-thinning fluids [7,26, 27,43,45,63,70,71,100]. The storage modulus (G') and the loss modulus (G") depict the elastic property and viscous property of ink, respectively. G' refers to the stored recoverable energy (elastic energy) during the shear deformation, and G" refers to the lost energy during the viscous deformation. A rotational rheometer is broadly used to measure the moduli, shown in Fig. 3(a). A high ink storage modulus (G') (in the order of 10<sup>3</sup>) enables sufficient shape retention of ink upon extrusion. The loss modulus (G") shall be smaller than the G' at lower shear stress, such that at the quiescent state, the elastic behavior dominates the plastic behavior. As the shear stress/shear strain increases, the cross-over point of G' and G" denotes the yield stress, indicating beyond this point, ink yields to the shear deformation, and the plastic behavior dominates the elastic behavior. The high stiffness and high yield stress of the ink are ideal conditions for the printability of the non-Newtonian ink [28,63, 1001.

#### 2.3.3. Photosensitive ink

The printable photosensitive ink includes the photo-curable component and the associated photoinitiator. The light absorber is often added to the ink to facilitate high-resolution printing. A customized photosensitive ink recipe could offer more degrees of freedom when printing the porous structure. In recent years, we've seen more and more research works customized the ink recipe, instead of directly using the commercially available photopolymer resin. Therefore, the printability characterization of photosensitive ink becomes more vitally important. The ink curing behavior, characterized by the light penetration depth, is essential to assess the printability of the photosensitive ink [79, 103-106]. Derived from the Beer-Lambert Law, the relation between the penetration depth ( $D_p$ ) and the curing depth of ink ( $C_d$ ) within a unit area is denoted

$$C_d = D_p \ln\left(\frac{E}{E_o}\right) \tag{2}$$

Where E is the light exposure energy, and  $E_{\rm c}$  describes the minimum exposure threshold to trigger the photopolymerization.

Specifically for a particle-loaded ink [62,82,84–86], penetration depth  $(D_{\rm p})$  could be largely affected by the loading volume fraction and light scattering. The Griffith and Halloran derived the dependence between the penetration depth and light scattering for particle loaded ink,

$$D_p = \frac{2}{3} \frac{d}{\widehat{O}} \left( \frac{n_0^2}{\Delta n^2} \right) \tag{3}$$

Where *d* is the averaged particle size,  $\hat{Q}$  is the scattering efficiency,  $n_0$  is the refraction index of the plain photosensitive ink,  $\Delta n$  denotes the refraction index difference between the particles and the plain ink. The printable ink requires the curing depth  $(C_d)$  to be greater than the layer thickness to ensure the shape integrity. Song et al. [79,104,105] provided a comprehensive summary of the curing depth of particle-loaded photosensitive inks. A prism spectrometer can be used to measure the refraction index of the solid particles and liquid ink. A rule of thumb for designing the photosensitive ink is to have high solid loading and low viscosity as much as possible. A high loading promotes high green density, which eventually results in a high yield. A low viscosity ensures fewer cracks and high homogeneity in the microscale structure. Zhang et al. [107] found that adding dispersant to the ink could help to tune the printability towards high loading and low viscosity. The effectiveness of a series of dispersants was examined, the result showed that dispersant KOS110 could facilitate high alumina particle loading (60 vol%), and the ink also presented low viscosity (15.4 Pa s).

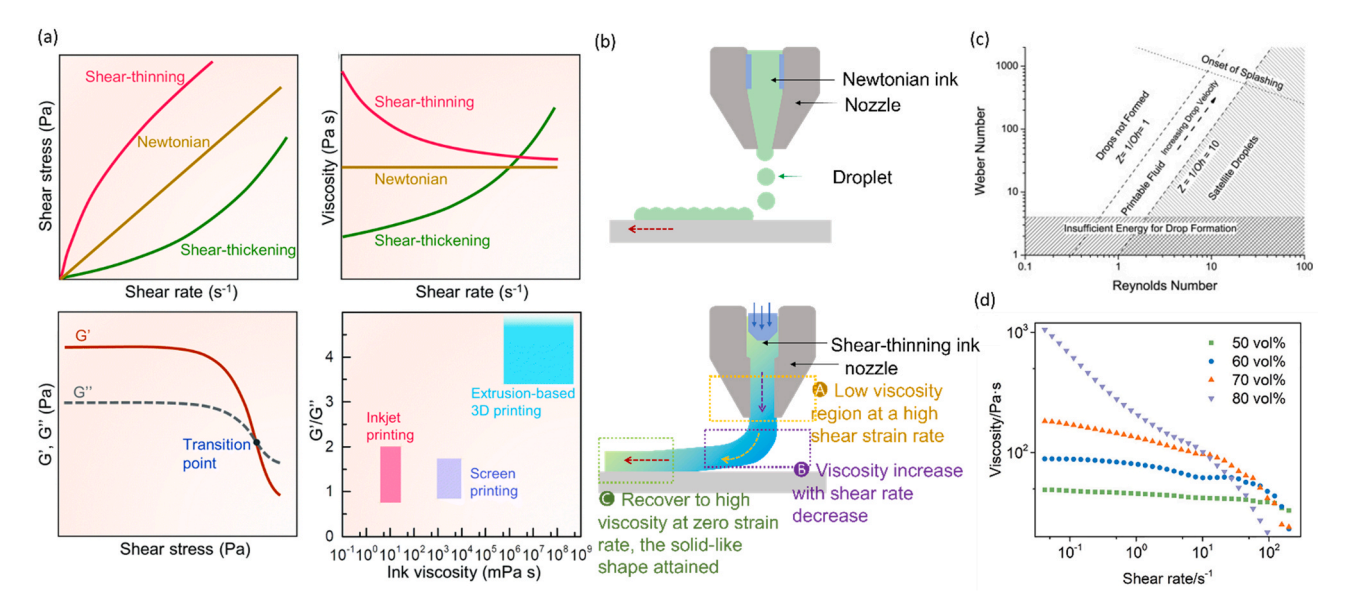


Fig. 3. Ink printability. (a) An illustration of rheology properties of Newtonian and non-Newtonian ink. (b) Schematic of jetting of Newtonian ink and extrusion of non-Newtonian ink. (c) Mapping the Ohnesorge number (Oh) with the jetting behavior. (d) An example of tuning the rheology behavior towards shear-thinning property. The increasing loading concentration of solid particles (building block materials) promotes the shear-thinning property of ink.
(a) Reproduced with permission [101]. Copyright 2021, Royal Society of Chemistry. (c) Reproduced with permission [102]. Copyright 2011, ELSEVIER. (d) Reproduced with permission [65]. Copyright 2020, ELSEVIER.

#### 3. Additive manufacturing processes

#### 3.1. Inkjet printing

Inkjet printing is a drop-on-demand and non-contact ink deposition process. The Newtonian ink is jetted from a piezoelectric actuated nozzle, and form droplets in the scale of micrometers. This promising technique is capable of printing complex geometries with high shape fidelity and resolution, realizing applications across energy storage [17, 62], flexible and wearable device [108-110], solar cells [111], sensors [112-114]. There's a clear trend that whenever a rapid patterning (in two-dimension) of material is required, inkjet printing is a preferred process, owing to the easy-accessible printing equipment, low-cost and high resolution. Lübkemann et al. [31] filled the Cadmium selenide (CdSe) ink to a commercial inkjet printer cartridge. The printed material was then dried under a supercritical CO<sub>2</sub> environment to obtain a highly porous structure. A drawback of using a commercial printer is the lack of the degree of freedom to change the process parameter. As a result, in their work, the printing time was prolonged to the order of minutes even hours for accurate printing. To prevent the undesired in-situ gelation during the long printing time, they added the destabilization agent (H<sub>2</sub>O<sub>2</sub>), Hydrogen peroxide to a second cartridge. The destabilization agent was subsequently mixed at the nozzle before jetting. During the printing, it's also important to create a moist environment around the printer to prevent nozzle clogging due to fast solvent evaporation. In this case, the authors maintained the humidity at 70% [31]. With a commercial inkjet printer, a true three-dimensional (3D) porous structure can be barely fabricated. Therefore, in many works, researchers custom-built the inkjet printer. Zhang et al. [18] invented the freeze nano printing (FNP) technique and fabricated the true 3D porous graphene aerogels for the first time. The technique combined the inkjet printing and freeze-drying process. The Newtonian graphene oxide ink was deposited with a drop-on-demand printer, a second nozzle was used to jet the pure water, the water drop was rapidly frozen to ice crystals on a cold substrate (-25 °C). Ice was created as a sacrificial material to support the overhung region during the printing, and was sublimated during the freeze-drying process. This technique is capable of creating multi-scale pores from micron size to millimeter size. The micron-sized pores are generated by removing the individual ice crystals, the pores

are in a laminated pattern. The millimeter-sized pores (lattice structure) are fabricated by removing the supporting ice. With the multi-scale porous structure, the printed graphene oxide has ultralight bulk density and high specific surface area. Due to the seamless combination of inkjet printing and freeze-drying, the FNP technique was then broadly used to print many other functional materials, follow-up works include process parameter study [29,115], quality control study [97,116], printing graphene oxide-ammonium thiomolybdate composite [17], printing silver nanowire aerogel [117], printing graphene oxide-ceramic composite [118].

The integrity of the printed object is one of the most critical considerations for inkjet printing of porous structures, as it ultimately determines the functionality of the porous structure. Specifically, how to ensure the proper bonding between the adjacent droplets and layers is of great importance. The most straightforward way is to directly print the material on a substrate [17,20]. This method is widely used for printing two-dimensional structures on the flexible substrate [13,119,120] and conductive substrate [13,20,22]. Material handling, post-processing and characterization can gain benefits with an appropriate substrate. For the 3D structure, the hydrogel bonds and  $\pi$ - $\pi$  interaction play a key role in binding. When the newly deposited drops and layers contact the previous not-yet-solidified material, the hydrogel bonds can be formed between the droplets and layers. In the FNP technique, on top of the hydrogen bonding, the in-situ ice crystal growth penetrates to the layer boundaries, squeezing the graphene oxide sheets to contact tighter and stack closer, thereby forming the  $\pi$ - $\pi$  interaction [18,121,122]. Gelation during the inkjet printing can also ensure structural integrity, as the cross-linked network can be formed from the gelation and serve as the skeleton of the printed sample [31,120]. If none of the abovementioned methods can facilitate binding in certain circumstances, adding a binder material can potentially reinforce the strength. Binder material crosslinks its own network to encapsulate the building block material. Using a binder could diminish the material performance, thus an extra post-processing step to remove the binder after printing may be essential Fig. 4.

#### 3.2. Extrusion-based direct ink writing

The extrusion-based direct ink writing (DIW) technique leads the

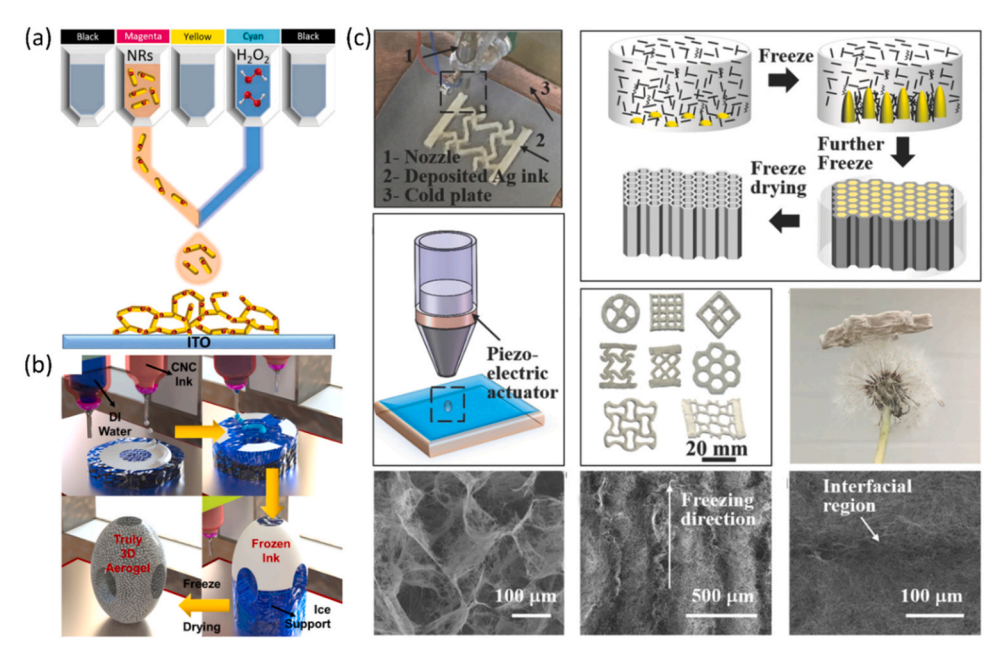


Fig. 4. The inkjet printing process for porous structures. (a) Schematic illustration of a multiprint-head setup, the deposition of various materials via drop-on-demand jetting enables the in-situ gelation. (b) Schematic of the inkjet printing with the freeze casting process, ice is used as support material to obtain truly 3D architecture. (c) 3D inkjet printing of silver nanowire aerogels.

(a) Reproduced with permission [31]. Copyright 2019, Wiley. (b) Reproduced with permission [123]. Copyright 2021, ELSEVIER. (c) Reproduced with permission [117]. Copyright 2017, Wiley.

trend of 3D printing porous structure. As a highly programmable and customizable 3D printing platform that can assemble 2D and 3D material into multi-scale, DIW creates 3D porous structure with a wide range of applications, including thermal insulation [7,124,125], water purification [4,126], battery and supercapacitor [70,127-129], optical device [130,131], electrical device [132,133], artificial bone scaffold [9, 134-137] and catalysis [138,139]. Compared to inkjet printing, the DIW technique is less challenging in terms of ink preparation and equipment construction. It functions by extruding the non-Newtonian ink from the nozzle, where the nozzle path is predefined by the G-Code files. The typical nozzle size varies from 0.05 mm to 2 mm. The extrusion methods include pneumatic pressure extrusion, mechanical extrusion, pneumatic-powered plunger extrusion, and screw extrusion. The versatile DIW can produce customized structures with high resolution. Combined with an appropriate post-processing method, multi-material and multi-porous structures with multi-functionalities can be obtained.

Multi-scale and hierarchical porous structures offer a combined ascendancy of low density and high relative compressive strength. The human bone scaffold, bamboo, wood, and many natural materials possess this superior porous structure. DIW method can create patterned porous structure (micro-lattice structure) in the scale of tens of micrometer to millimeter. Coupled with the sol-gel pre-process and the supercritical drying post-process, DIW can produce macro-porous structures with nanometer-sized pores. Zhao et al. [55] first printed the silica aerogel using the abovementioned strategy. Owing to the multi-scale porous structure, the specific surface area can reach 751 m<sup>2</sup>/g, with an ultra-low thermal conductivity of 15.9 mW/mK. Chandrasekaran et al. [140] explored the DIW of organic and carbon aerogels lattice derived from the resorcinol-formaldehyde sol-gel process, coupled with supercritical solvent extraction. A phenomenon high surface area (greater than 2000 m<sup>2</sup>/g) can be obtained in the printed carbon aerogel lattice. The size of the nano-scaled pores created by the sol-gel process is around 2 nm, while the size of the micron-scale pores created by the DIW is around 200 µm. Similarly, 3D printed graphene aerogel micro lattice was reported in [73,74] and cellulose nanocrystal aerogel in [141]. Maleki et al. [142] 3D printed the silica-silk fibroin hybrid aerogel in lattice structure using the DIW and dried with supercritical CO<sub>2</sub>, and the final product possesses a low density and excellent flexibility in compression (up to 80% strain). These works highlight the combination of DIW with supercritical drying for creating multi-scale porous structures. Such structures have significantly outperformed the bulk counterpart and thereby enabling a boost in their performance. Freeze-drying was combined with DIW to fabricate highly porous LiFePO<sub>4</sub> [77]. A freezing agent (1,4 dioxane, melting point at 11.8 °C) was used to solidify the ink upon extrusion and maintain the free-standing 3D structure. Coupled with the freeze-drying process, 50–200 µm pores can be developed. A significant enhancement in the transportation of Li-ions was observed in the macroscopic porous electrode compared to the bulk counterparts. The benefit of including such phase-change material (1,4 dioxane [77], glacial acetic acid [76], DMSO [37], and camphene [75]) in DIW is that the thermally-triggered phase-change phenomenon can help to in-situ solidify the just-extruded ink, which can relax the printability requirement of the prescribed non-Newtonian ink (Section 2.3.2). Low viscous ink, with higher concentration of solvent/ templating material can be printed, paving the way to reach higher porosity of final product.

A higher level of the multi-scale porous structure can be produced with sacrificial templating and emulation templating. Pore size can be previously manipulated by controlling the size of the sacrificial beads and emulsion beads. Huang et al. [65] demonstrated DIW with PMMA (Polymethyl methacrylate) sacrificial bead can generate a multi-scale hierarchical porous structure with pore size ranging from  $0.5~\mu m$  to  $200~\mu m$ , and the concentration of sacrificial beads can control the porosity. Sommer et al. [143] added wax and konjac gum as the sacrificial templates to fabricate hierarchical silk fibroin structure. Because the spherical pores yield the highest surface area, the water-oil emulsion and foaming methods can serve this purpose. The oil drops from emulsion [56–59,61,144] or gaseous bubbles [7,63,68,145] from foaming are introduced in the ink as an external phase component. As described in the Section 2.2.2, those stably dispersed drops/ bubbles can ultimately form the spherical porous structure.

The merit of DIW has further been explored to print multi-material in one object, leading to multi-functional product fabrication. Multi-functionalities of porous structures are essential in many applications. For example, the bio-medical application requires the printed part to have necessary mechanical properties as well as biological properties [3, 137,146]. Ruiz-Cantu et al. [146] printed the porous PCL (polycaprolactone) and GelMA (gelatin methacrylate) scaffold for nasal reconstruction. As a biocompatible and biodegradable material, PCL offers the printed sample with robust mechanical properties. GelMA is a widely used biopolymer that provides a suitable environment for cell viability. Two feedstock materials were prepared to non-Newtonian ink,

respectively. A multi-nozzle extrusion printer configuration was used, each ink is printed to the pre-defined region or layer. Ortega et al. [124] proposed active mixing of multiple materials to reach the local homogeneity of disparate inks. The method is implemented using a micro impeller mixer at the nozzle, and the mixed ink was then deposited using a single nozzle. The rheology of the mixed inks and their fluid dynamics properties were investigated. A near-continuous change in the volume fraction between the two inks can be achieved, thus the printed part demonstrates a spatially gradient change in the thermal conductivity.

DIW technique as a scalable and cost-effective method, when producing the porous structure, can potentially address environmental issues elevated in the conventional manufacturing processes. Compared with the molding and machining processes, DIW can build parts ondemand by adding materials to avoid waste. Though the removal is required in the sacrificial templating process, the successful use of environmentally friendly organics (sunflower oil [58] and corn oil [59]) as the templating material paves the way for sustainable manufacturing. In this regard, the DIW combined with the direct foaming method [7] requires the least energy, material, and time consumption.

#### 3.3. Stereolithography printing

Stereolithography printing (SLA printing) is one of the earliest developed rapid prototyping techniques, it offers fast and highresolution printing by using laser [82,104,147,148] or mask-image based [81,85,86,92,105,149-153] light irradiation to selectively solidify the photosensitive ink. Bottom-up and top-down are two main configurations in SLA systems. The light source is placed underneath the ink vat and the printed part is built facing upside down. Bottom-up configuration is widely used as it requires less ink and can achieve the finest features. Sun et al. [92] used bottom-up SLA combined with the freeze-drying process to 3D print PEGDA (polyethylene glycol diacrylate)-CNF (cellulose nanofibril) aerogels. PEGDA is miscible with water, with the addition of initiator (Eosin Y disodium salt (eosin Y), triethanolamine (TEA), and 1-vinyl-2 pyrrolidinone (NVP)), it serves as the photocurable component in the ink. The freeze-drying process sublimates water, and thus generates the porous scaffolds. Because the porous scaffolds lack mechanical strength, CNF was added to the ink accordingly to mitigate this shortcoming. This method is also adopted by [153] to 3D print micro-architected graphene aerogels and dental bridges [82]. Aubert et al. [84] presented another successful confluence of nanomaterial synthesis and additive manufacturing to print nanomaterials with nanoscale porous structures. The sol-gel synthesis of nano-porous "cage" silica was integrated into the SLA printing coupled with supercritical drying. The high-resolution and shape fidelity were accomplished by the SLA technique, and the nano-sized porous structure has great potentials for catalytic, sensing and energy applications [2].

The photocurable component PEGDA has good mechanical strength that can overcome the suction force incurred during the pulling-up movement in a bottom-up configuration. A large suction force at the interface between the cured part and the vat glass-bottom could potentially damage the printed part [152]. That's also one of the deciding reasons that PEGDA is a favorite ingredient in photosensitive ink. An alternative approach to avoid the suction force damage is using the "Top-Down" configuration, where a light projector is located above the ink tank, and the build platform moves downwards during printing [82,84,104]. Top-down configuration can handle large-scale printing, and because the cured part sits on the platform, the process is less prone to failures.

Highly viscous ink has also been printed on custom-designed SLA printers. Due to the poor mobility of the viscous ink, it requires an external force to refill ink to the center region of the tank. To conquer this challenge, Song et al. proposed the SLA process integrated with tape casting method, where a doctor blade was swept across the ink top surface, spreading a new layer in the printing area [81,85]. This method is used to print porous structures with sugar as the foaming agent. Sugar

was uniformly mixed with the photosensitive ink before SLA printing, it was then leached out in hot water after printing, left the space with empty pores [85]. A similar blading method was adopted by Mu et al. [86], where a rotational blade was used to recoat the printing area for each layer. The photosensitive ink contains salt as the sacrificial template for porous structure, different sizes of salt particles were added to the ink, resulting in a multi-scale porous structure. PEGDA was used as the photocurable ingredient in the ink, with its miscibility in water, the printed structure gained the shape memory effect triggered by temperature change. Such porous hydrogel structure with shape memory effect has promising potential for drug delivery application Fig. 5–9.

#### 4. Post-processing methods

A post-processing procedure is required for most as-printed samples to gain the designed porous structure and the functionalities. The sacrificial templates, polymeric binders, and other impurities are removed/decomposed during the post-processing.

#### 4.1. Solvent exchanging

Solvent exchanging is the most advanced and effective way to create porous networks. Typical solvent exchanging methods include supercritical drying, freeze-drying, and ambient drying, all widely used in industrial production. Supercritical drying operates with supercritical fluids, the supercritical  $\rm CO_2$  (critical point 31.1 °C at 1072 psi) is mainly used among all the fluids. At the critical point, the phase distinction (phase boundary) between the liquid and vapor vanishes, thereby the surface tension and the capillary stress of solvent largely decrease [155]. The nanometer-sized porous network is thus obtained without pore collapsing [91], which also ensures the ultrahigh porosity (greater than 90% in [142]) and low density (less than 0.1 g/cm³ in [73,74,91,140,142,153]) of the printed parts. The drawbacks of the supercritical drying process are the high equipment cost, high energy consumption, and limited porosity tunability.

Freeze-drying takes a similar route by sublimating frozen solvent to vapor under low pressure. The frozen solvent crosses the phase boundary from solid to vapor and bypasses the liquid phase, the capillary stress is thus refrained. The deep vacuum (pressure less than 0.05 mBar) builds a negative pressure environment, providing the continuous driving force to evict the solvent out from the samples. As the most natural, clean, and abundant liquid material on the earth, water is widely used as the solvent for freeze-drying. The size of the ice crystals determines the pore size in the final product, usually in a micrometer scale. Therefore, it is favorable to employ a fast-frozen rate to avoid unwanted large ice crystal growth. A most common practice is dipping the just-printed sample to liquid nitrogen or placing the sample in the freezer [17,18, 76,77,82,117,118,156–158]. By manipulating process parameters such as the freezing temperature, pressure, and frozen rate, the porosity of the final product can be rationally controlled [159,160]. Shrinkage (around 10%) is often observed on the freeze-dried samples, in that most solvents have a higher density in the solid phase than in the gas phase [161]. Compared with supercritical drying, freeze-drying is less expensive in terms of equipment and processing time, but it suffers from scalability and energy consumption issues.

Ambient drying does not involve high-precision equipment, and the solvent directly crosses the phase boundary from liquid to gas and volatilizes from the printed sample under ambient pressure. High volume loss usually happens during the ambient drying because of the surface tension at the solid-liquid interface pulls the neighboring structure together. 3D printing can play an important role in preventing large shrinkage even cracks by fabricating a sophisticatedly designed structure. With a triply periodic minimal surface structure (TPMS structure) or hollow lattice structure, the printed object has a larger contact area with air, facilitating uniform solvent volatilization [6,61,162]. Besides the printed geometry, a low-surface-tension solvent is more suitable for

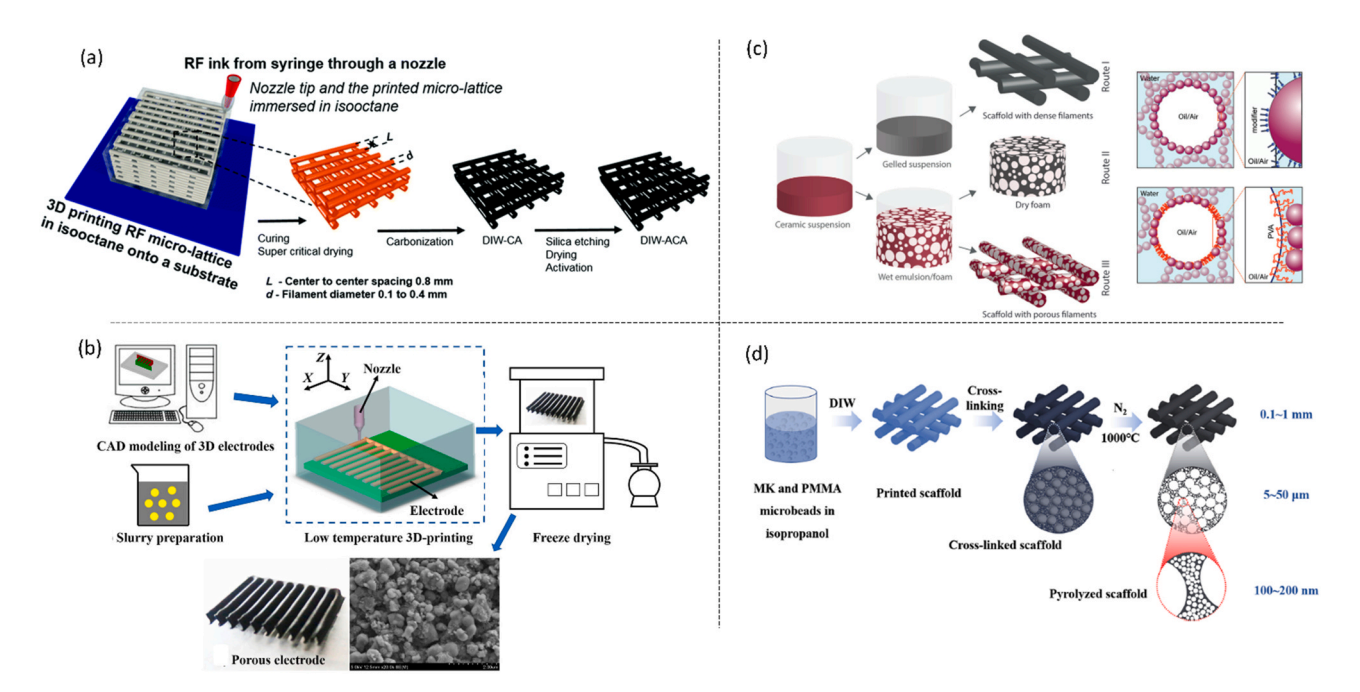


Fig. 5. Direct ink writing printing process for porous structures. (a) Schematic illustration of DIW carbon aerogels coupled with supercritical drying. (b) Schematic of DIW LiFePO<sub>4</sub> electrode in low-temperature environment. The freeze-drying process is carried out to eliminate the solvent and creates the porous electrode. (c) An oilwater emulsion approach is applied to DIW for creating spherical pores. (d) A sacrificial templating approach for creating 3D multi-scale porous structures. (a) Reproduced with permission [140]. Copyright 2017, Royal Society of Chemistry. (b) Reproduced with permission [77]. Copyright 2017, MDPI. (c) Reproduced with permission [61]. Copyright 2016, Wiley. (d) Reproduced with permission [65]. Copyright 2020, ELSEVIER.

ambient drying [12]. The alternative path is to form an additional network that superimposes the porous network. This network needs to have sufficiently high strength to overcome the capillary force and surface tension during ambient drying to protect the porous structure. The addition of polymeric binder material or fiber in the ink can form such reinforcing network. This approach has been adopted to dry 3D printed alumina in porous structure [61,63], cellulose nanofiber aerogel [163], porous silica [162], and silica aerogel [7]. Ambient drying is an efficient and cost-effective approach, and it's suitable for large-scale manufacturing of micron-size to millimeter-size porous structures.

#### 4.2. Sacrificial template removing

A carefully designed sacrificial template removing process guarantees the ideal porous structure to be achieved. Based on the property of sacrificial material, two types of methods, heat treatment, and leaching are broadly used. Heat treatment burns out the sacrificial material at high temperature. It's primarily compatible with ceramic building blocks due to the outstanding heat resistance of ceramics. A thermogravimetric analysis (TGA) shall be carried out beforehand to develop a temperature profile for the heat treatment [59,65].

Sugar [85], sodium chloride [86], copper sulfate [164] salt, and Konjac gum [143] have good miscibility in water, therefore they were removed by dipping the as-printed samples in water, dissolving the templating materials into the water. These water-soluble sacrificial materials are preferable candidates for biomedical applications. Chemical assisted leaching was used in [143], where wax beads were dissolved in dichloromethane (DCM). Hot KOH solution (Potassium hydroxide solution) was used in [78] to remove the silica nanosphere (etching for 3 days). These washing/etching methods are usually repeated several times for the complete removal of sacrificial materials.

#### 5. Morphology of the printed porous structure

The pore shape, size, and distribution can be rationally designed in versatile AM processes for a porous structure. Performance-driven pore morphology design ensures the printed porous structure has the targeted functionalities and applications. This section discusses various pore morphologies realized by combining AM process and conventional post-processing techniques, sheds light on the applications in Section 6.

#### 5.1. Pore shape

Pore shape can be formed in regular geometries (spherical, planar) or irregular format, and the pores can be either in an aligned pattern or in a stochastic pattern. Spherical pores have the largest possible unit surface area compared to other shapes. Water-oil drops in emulsion ink [57,59,61], gaseous bubble in foamed ink [7,63,145], and sacrificial microbeads [65,143] in ink are favorable methods to create such spherical pores. The spherical pores are the ideal candidate for lightweight loading, thermal insulation, acoustic insulation applications.

The freeze-drying-based process is promising for producing planar shape pores [17,18,75–77]. Through controlling the freezing rate and freezing temperature [165], the fine-tuned laminar pore morphologies can be tailored. The external force fields [166] acting on printed samples during the pre-freezing step can achieve the locally or globally aligned planar pores. Directional and hierarchical pores can provide heterogeneous properties, which found tremendous opportunities in biomedical applications.

#### 5.2. Pore size

Different pore size can contribute to various applications. The nano-sized porous network is ideal for thermal insulation properties. Supercritical drying is mainly used for creating the nano-sized porous structure [55,74,140–142]. Multi-scaled porous structure has the pore size ranging from nanometer to millimeter, which can be formed by combining AM process and post-process method. AM processes (inkjet, DIW, SLA) can fabricate the interconnected porous network in hundreds of microns, whereas the post-process can fabricate pores in nanometer size. Hence, the integration of AM and post-process can synergically fabricate multi-scaled porous structures, finding various applications in

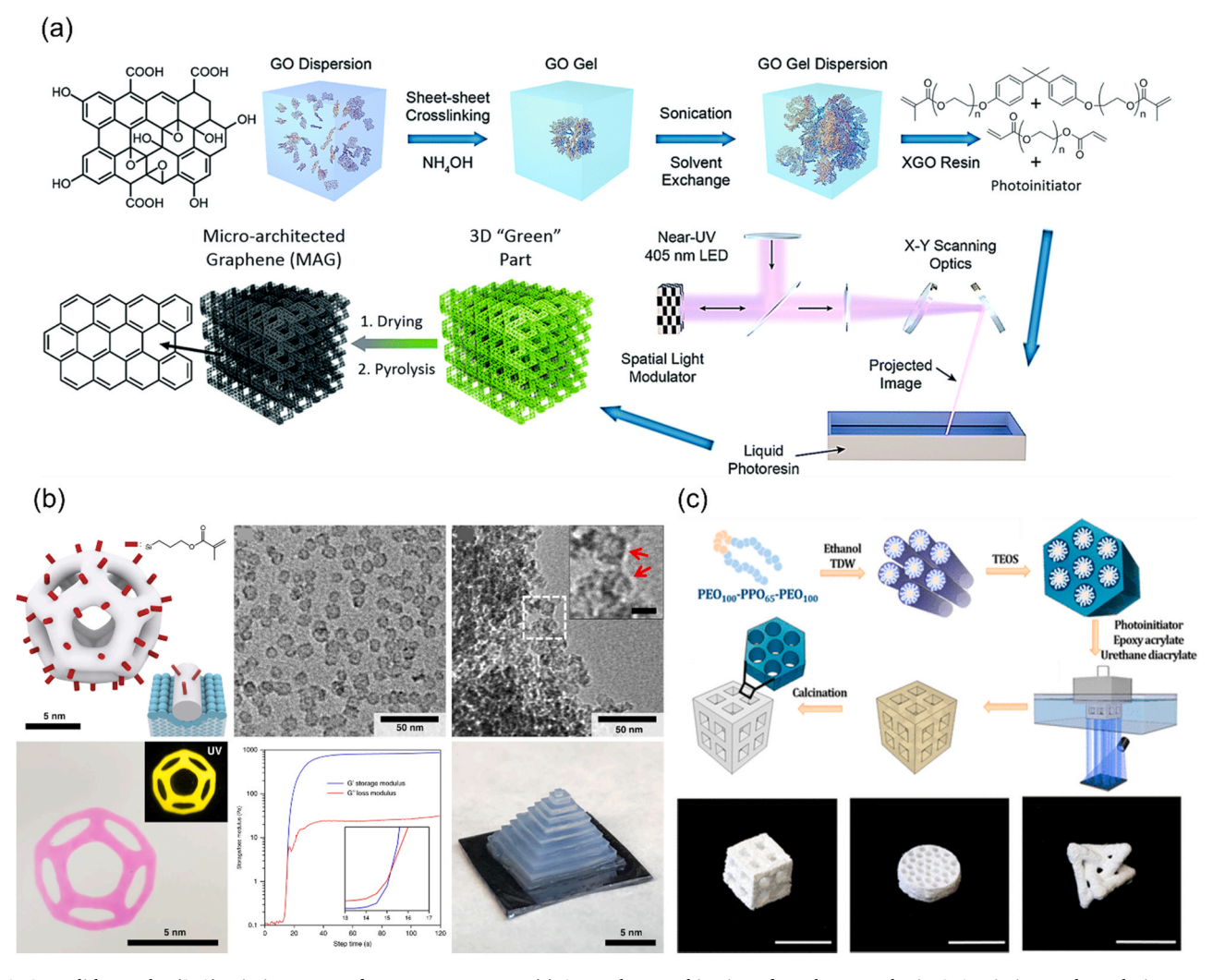


Fig. 6. Stereolithography (SLA) printing process for porous structures. (a) A seamless combination of graphene synthesis, SLA printing, and pyrolysis process for producing 3D multi-scale porous networks. (b) The sol-gel synthesis combined with SLA printing, and supercritical drying for fabricating the "silica cage" nano porous structure. (c) The ordered porous silica fabrication process. The integration of sol-gel synthesis, SLA printing, and calcination process enables the 3D printing of multi-scale porous structures (scale bars, 10 mm).

(a) Reproduced with permission [153]. Copyright 2018, Royal Society of Chemistry. (b) Reproduced with permission [84]. Copyright 2020, Springer Nature. (c) Reproduced with permission [154]. Copyright 2020, American Chemical Society.

tissue engineering, energy storage, and filtration.

The mechanical property of 3D printed porous samples can be designed or estimated with the pore size. Gibson and Ashby [170] derived the Young's modulus of a porous structure as:

For an open porous structure,

$$\frac{E_{porous}}{E_{solid}} = C \left( \frac{\rho_{porous}}{\rho_{solid}} \right)^2 \tag{4}$$

For a closed porous structure,

$$\frac{E_{porous}}{E_{solid}} = C \left( \frac{\rho_{porous}}{\rho_{solid}} \right)^3 \tag{5}$$

Where  $E_{solid}$  is the elastic modulus of material feedstock, and the relative density is denoted as  $\frac{\rho_{porous}}{\rho_{solid}}$ . C is a dimensionless coefficient, for an ideal open/closed porous network, C=1. Huang et al. [65] discovered that with a fixed porosity (80%), a smaller-sized porous network (0.46  $\mu$ m) had higher compressive strength than a larger-sized (25  $\mu$ m) structure. Small pore size results in a smaller strut surface area, which in turn leads to an enhancement of the strength. Similar findings were reported by Colombo et al. [66], Tarafder et al. [171] and Brezny et al. [172].

#### 5.3. Porosity of the 3D-printed porous structures

Porosity defines the volume fraction of empty spaces in the printed objects. Although attaining a higher porosity is the ultimate goal of fabricating porous structures since it can possibly maximize the associated performances. However, a high porosity may also exclude the 3D-printed objects with high strength and durability. To this end, two routes are discovered to balance the porosity and mechanical strength. Many works are dedicated to developing strategies for tuning the porosity of 3D-printed porous networks. Using the sacrificial templating method (varying the concentration of template materials [59,65,173]) or the direct foaming method [63,64,145] can achieve precise control of structural porosity of 3D printed objects.

For specific application-oriented porous structures, people find that controlling the porosity alone is not sufficient to achieve the desired performance. For example, thermal insulation requires high porosity and demands the pore size to be as small as possible. With a small pore size and high porosity, the free flow of air can be restricted, thus enhancing the thermal insulation performance. Supercritical drying is effective in creating nanoscale porous structures with high porosity. Recently, a "porogen" material was introduced in Dong et al. [91],

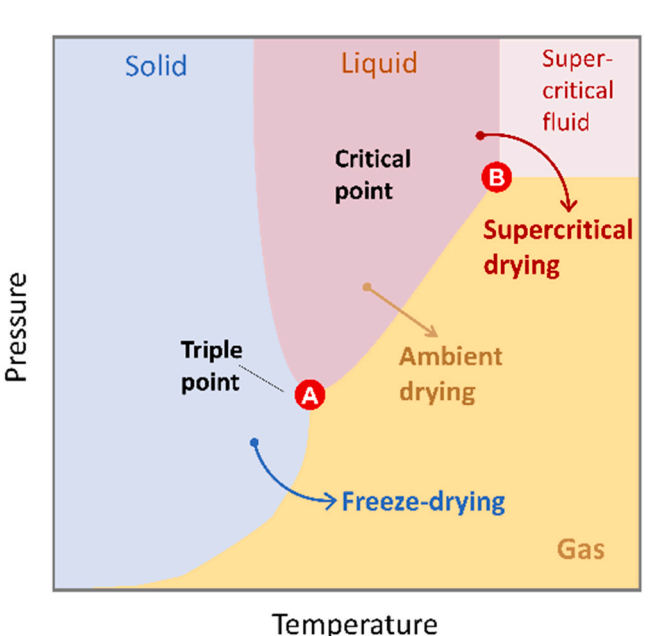


Fig. 7. Schematic phase diagram for solvent exchanging process.

which serves as a sacrificial material in the 3D-printed samples. The "porogen" can be removed during the supercritical drying, and the nanoscale pores can be generated. By changing the concentration of "porogen," the porosity can also be tuned to the desired level.

As indicated in Section 5.2, multi-scale porous structures comprising of nanoscale, micro-scale, and macro-scale pores grant the entire structure multi-functionalities. One approach to realize the wide variations in pore sizes within the 3D-printed sample is the introduction of hierarchical porosity, which can be largely observed in biological products, such as skin, bone, leaf, and tree trunk. The diverse functionalities of a multi-scale porous structure derive from the functional adaptation at all levels of pore hierarchy. Combining AM technologies and post-processing methods provides a facile tool for 3D printing the hierarchical porosity. 3D printing technologies can create macro-sized pores, and post-processing further generates micro-and nano-sized pores. The 3D-printed multi-scale porous structures provide an enhanced surface area, which proves to promoting energy density [2,18, 28,70,174], sensitivity [175], proton switching [90], adsorption efficiency [4,8,122], and cell attachment [152,176]. In the following section, we present more details of emerging functionalities realized by the multi-scale porous structure.

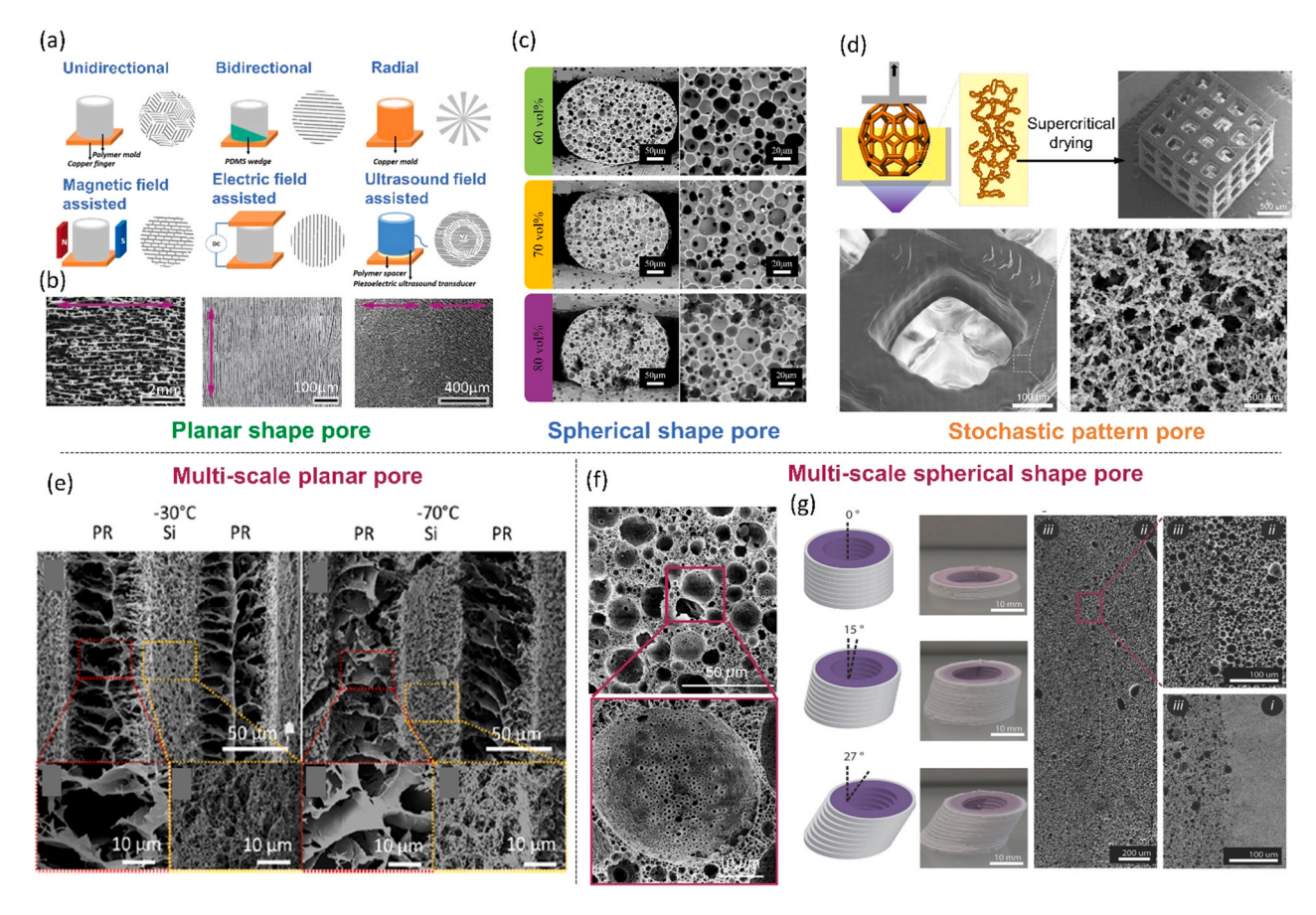
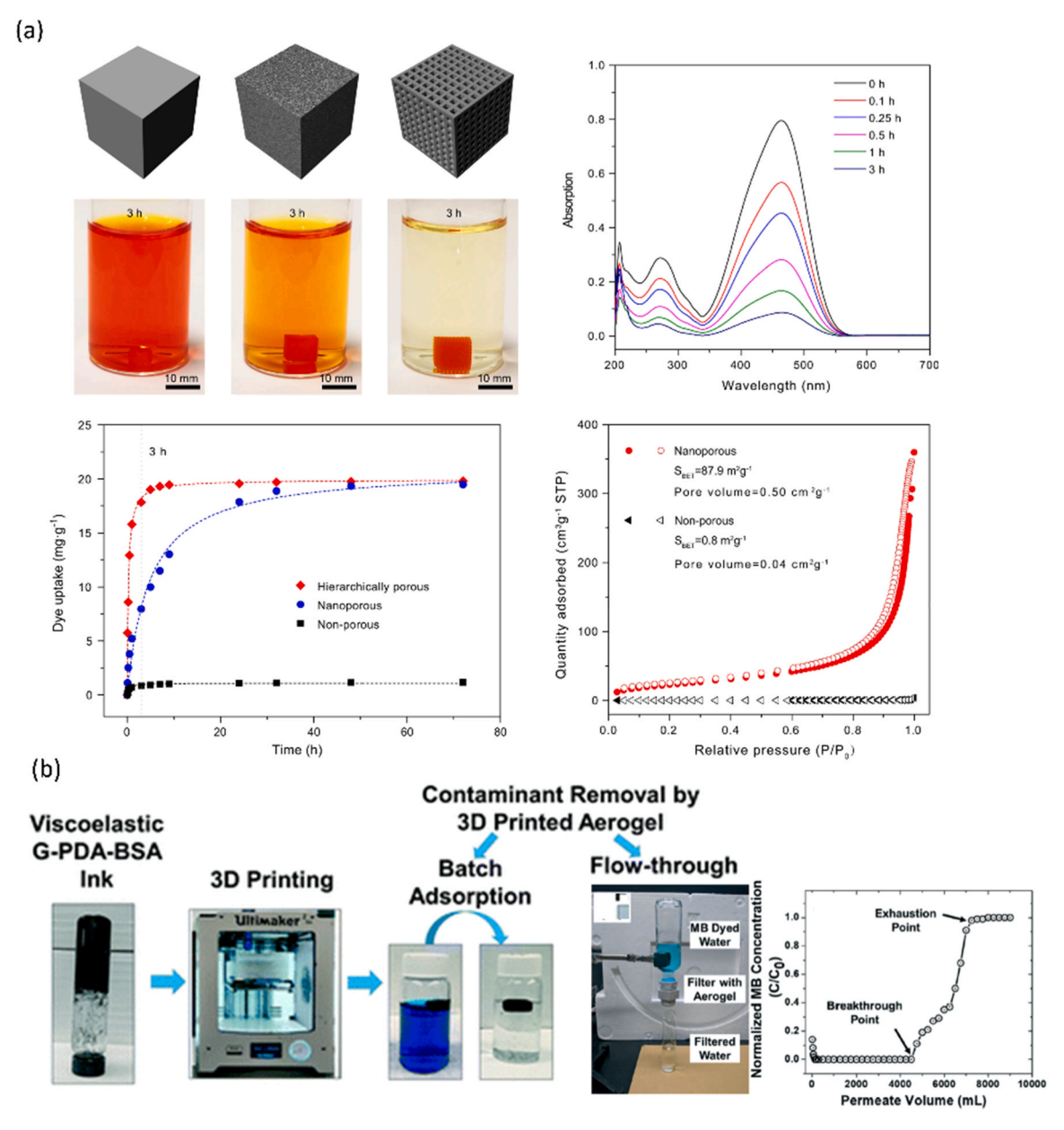


Fig. 8. Pore morphology. (a) Schematics of various freeze casting techniques for controlling the planar pore directions. (b) Examples of extrinsic control using energized fields during freeze casting. Fields used from left to right: Magnetic field, electric field, and ultrasound. (c) The spherical shape pores created with sacrificial microbeads. (d) The stochastic pattern pores (in nanoscale) created with supercritical drying. (e) Example of multi-scale planar porous structure, the pore size is controlled by using different freezing rates. (f) Examples of multi-scale spherical porous structures. (g) Examples of multi-scale spherical porous structures, produced by using two concentrations of oil-water emulsion.

(a) Reproduced with permission [167]. Copyright 2020, Wiley. (b) Reproduced with permission [168]. Copyright 2019, ELSEVIER. (c) Reproduced with permission [65]. Copyright 2020, ELSEVIER. (d) Reproduced with permission [91]. Copyright 2021, Springer Nature. (e) Reproduced with permission [169]. Copyright 2021, American Chemical Society. (f) Reproduced with permission [59]. Copyright 2019, Springer Nature. (g) Reproduced with permission [61]. Copyright 2016, Wiley



**Fig. 9.** Examples of pollutant removal applications. (a) A multi-scale porous structure significantly increases the surface area, promoting the adsorption performance of the 3D printed sample. (b) With the functional materials, the 3D-printed graphene oxide-based porous network can achieve flow-through filtration. (a) Reproduced with permission [91]. Copyright 2021, Springer Nature. (b) Reproduced with permission [4]. Copyright 2020, American Chemical Society.

# 6. Functionalities and applications – light in weight, heavy in application

With the flexible and versatile additive manufacturing techniques being extensively integrated into fabricating three-dimensional porous structures, the existing merits of the porous structure have been further magnified, offering more emerging opportunities and applications. "Light in weight, heavy in application" is even more obvious nowadays to describe the 3D printed porous structures. This section summarizes the most related and promising functionalities and developed applications of the printed porous structure. These state-of-the-art applications tackle environmental science, renewable energy science, and life science.

### 6.1. Filtration and pollutant removal

Water purification, wastewater treatment, pollutant removal, and

filtration have significant impacts in environmental applications for creating renewable resources and building a clean and green environment. Materials like graphene [8], graphene aerogels [177], and chitosan [5] are widely explored for pollutant absorption. AM techniques can play a leading role in further improving the filtration and pollutant removal efficiency by creating complex shapes for conformable devices. Owing to the outstanding processability for creating hierarchical multi-material and multi-scale pores, AM can achieve structures with large surface area. Consequently, the increased surface area of the porous structure increases the pollutant absorption efficiency. Masud et al. [4] reported direct ink writing (DIW) of a graphene-based ink, followed by freeze-drying to create graphene-biopolymer aerogel. The printed sample was tested for removing water contaminants, including heavy metals, cationic and anionic dyes, and organic solvents. Benefitting from the multi-material ink, the printed graphene-biopolymer aerogel outperformed the regular graphene oxide powder in the removal capacity by 3-4 times higher. Furthermore, an 80-90% removal

efficiency was discovered in the cycling test, suggesting the printed graphene-biopolymer aerogel has promising potential for tap water flow-through filtration and bottle-cap water filtration. The conformal shape for these filtration systems can be easily manipulated and printed by using AM techniques. Zhang et al. [178] printed the chitosan ink for heavy metal ion absorption and removal. Chitosan is a biological absorbent, which has the intrinsic polymer chelation property. With the high-resolution SLA printing, a fine honeycomb lattice structure can produce a large surface area, promoting the contacting area of chitosan (with amine and hydroxyl group) and heavy metal ions. Therefore, the 3D printed chitosan porous structure gains a larger capacity to absorb heavy metal ions in water than that of the regular chitosan flakes. During the SLA printing, a robust polymer network was formed and assembled with the chitosan building blocks. This durable network ensures the printed sample maintains the as-printed structure, even after cycles of absorption and desorption. Besides, the durability further prevents the sample from degradation in a harsh environment (acid or alkaline environment) or in high-temperature conditions (up to 100°C).

Dong et al. [91] proposed a generic AM approach to creating structures with open, nano-sized pores for pollutant removal. A novel polymerization-induced phase separation method was integrated into SLA printing, coupled with supercritical drying. The micrometer-sized pores can be formed using SLA printing, and it prompts the mass transfer, resulting in a 20-times higher uptake of organic dye in water. Moreover, the nanometer-sized pores are superimposed to the macroscopic lattice, which significantly increases the surface area, and in turn provides capillary tension for adsorption. As a result, the sample can effectively remove the organic dye, and no structural degradation was observed over time. The findings from this paper highlight the advantage of combining the AM process with traditional porous structure manufacturing. The versatile nano-porous network is capable of decontamination without relying on the specific carbon-based adsorbent material.

#### 6.2. Energy storage

Energy storage devices such as batteries, supercapacitors, and triboelectric nanogenerators are acclaimed as attractive clean energy technologies. The way of structuring the active material feedstock can primarily affect the performance of the energy storage devices, and the flexible AM techniques bring immense benefits in this regard. 3D printed energy storage devices in porous structures can enhance the capacitance, sensitivity, and efficiency, compatible with flexible and wearable devices. The performance of porous 3D printed energy storage devices can significantly outweigh their bulk counterparts. Research works on printing the rechargeable lithium-ion batteries were reported by Cao et al. [100], and the sodium-ion batteries by Brown et al. [17]. It is found that the 3D printed multi-scale porous structure can enhance the battery cycling performance (more than 85% of the initial capacity can be maintained after 3000 cycles) and increase the specific capacity. The improved performance is mainly attributed to the abundant ions within the large surface area porous structure, which provides high accessibility to the electrolyte. Fu et al. [179] developed graphene oxide-based electrode inks for direct ink writing of lithium-ion batteries. Graphene oxide was mixed with Lithium iron phosphate (LiFePO<sub>4</sub>) for printing cathode, and mixed with lithium titanium oxide (Li<sub>4</sub>Ti<sub>5</sub>O<sub>12</sub>) for printing anode. Followed by freeze-drying, the flake-like porous structure creates a large surface area to house the electrolyte. The final fabrication step is to fill the electrode channel with solid-state electrolyte, forming a fully packed rechargeable lithium-ion battery. A high initial charge capacity (117 mAh/g) and discharge capacity (91 mAh/g) with excellent cycling stability can be achieved. The addition of graphene oxide ensures the favorable electrical conductivity of a highly porous structure and promotes electrochemical performance. Similar GO-based ink for printing porous sodium-ion batteries was also reported in [157].

Graphene oxide-based porous networks can be thermally or

chemically reduced to graphene-induced porous networks, further improving the electrical conductivity. Such activated materials are ideal candidates for producing supercapacitors [180]. Zhu et al. [73] demonstrated the 3D printed graphene-based micro-supercapacitor. Over  $700 \, \text{m}^2/\text{g}$  of surface area was obtained with direct ink writing followed by supercritical drying. A multiscale porous network ensures the high throughput of ion diffusion through the thick electrode. Specifically, the ordered macropores printed by DIW improved the infiltration of gel electrolytes, thus promoting the mass transfer. Moreover, the addition of graphene facilities the charge transfer. In turn, the 3D printed micro-supercapacitor exhibited a low internal resistance and sizeable gravimetric capacitance. The performance remains high efficacy (95.5%) after more than 10,000 consecutive charge and discharge cycles.

Flexible and wearable electronics are gaining lots of attention in recent years, it's becoming a viable pathway for the smart electronic era. Most of the existing flexible textiles are directly built on the soft and planar substrates. However, many flexible substrates possess a large resistance, it is therefore posing challenges to fabricate flexible supercapacitors with high energy density. The hydrophilic graphene oxide can be easily prepared to aqueous GO ink, which is favorable for the inkjet printing. Inkjet printing enables depositing numerous carbonbased active materials onto planar and soft substrates. Moreover, owing to the drop-by-drop depositing principle, a better percolation of the active material on the textile substrates can be achieved, which in turn contributes to an improved conductivity. Based on this innovation, many 3D printed flexible supercapacitors were developed. Chen et al. [181] printed the hybrid carbon nanotube/RuO<sub>2</sub> on a cloth substrate. Two inkjet-printed films and a solid electrolyte were subsequently sandwiched together to form the flexible supercapacitor. The ruthenium oxide (RuO2) was added to ink to promote electrical conductivity, resulting in a higher power density of 96 W/g and an energy density of 18.8 mWh/g. Similar works were reported by Choi et al. [16] for inkjet printing supercapacitors on paper, and by Jung et al. [182] for printing the graphene on a series of soft substrates, which demonstrates the generality of 3D printing supercapacitors with porous structures. Furthermore, their work reveals the printed supercapacitor can retain the performance even with large deformation (180-degree bending).

#### 6.3. Thermal insulation

Diffusion is the inherent nature of thermal energy, therefore, thermal insulation is critical for reducing energy waste and thus improving energy efficiency. Materials with intrinsic low thermal conductivities are widely used for industrial applications. Additive manufacturing techniques can be seamlessly combined with conventional porous material synthesis, creating shape-conformable, large-surface area, and ordered porous structures. An enhanced thermal insulation performance can be realized with a 3D printed multi-scale porous structure.

Low thermal conductivity of porous network originates from the constrained heat transfer across the gas phase, which is confined within the pores. In other words, the internal pores or voids break the continuity of heat transport, therefore lowering the thermal conductivity. Based on this design principle, Farrell et al. [154] reported SLA printing combined with sol-gel process for producing multi-scale porous structure. The highly ordered nanometric pores are favorable for restricting the heat transfer. Coupled with the 3D printed lattice micrometric structure, the specific surface area (around 1900  $\rm m^2/\rm g)$  and porosity were further increased.

The extrusion-based direct ink writing also features the capability of creating miniaturized and complex shapes. Zhao et al. [55] printed pure silica aerogel using DIW with supercritical drying. The printed sample exhibited an ultralow thermal conductivity of 0.0159 W/m K, with a conformable shape designed for electronic thermal insulation. Guo et al. [7] printed silica aerogel in various free-standing 3D shapes (Fig. 10(a)), the thermal insulation behavior was investigated for different models

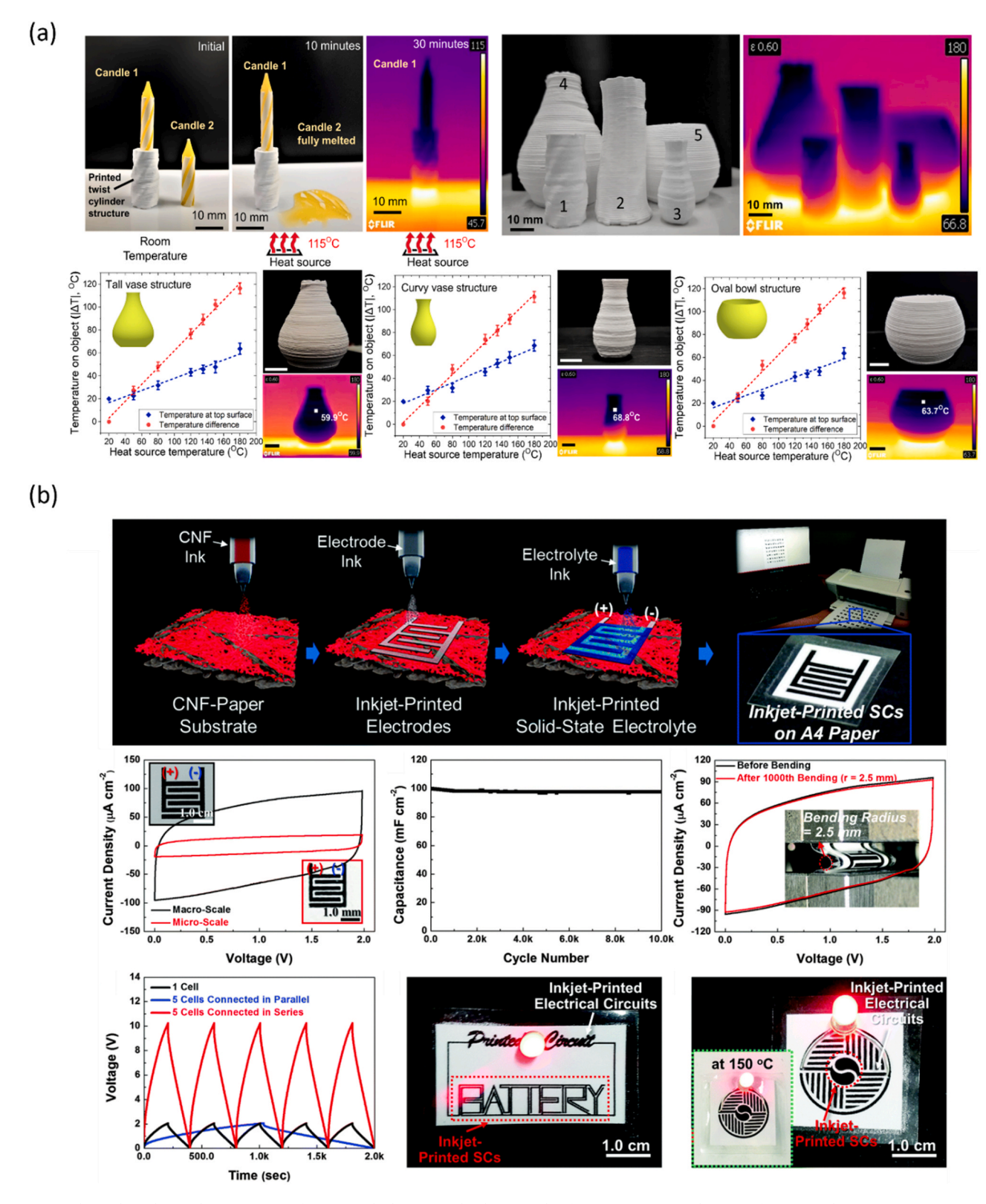


Fig. 10. (a) Thermal insulation demonstration of 3D-printed silica aerogels. (b) Example of energy storage application of 3D-printed porous structure. (a) Reproduced with permission [7]. Copyright 2021, American Society of Mechanical Engineers. (b) Reproduced with permission [16]. Copyright 2016, RSC.

and in different temperature environments. The results indicated that all the 3D-printed aerogel objects could achieve the same thermal insulation performance, regardless of the geometry and the environmental temperature. The silica aerogels are preferable candidates for thermal insulation applications, however, the insufficient interparticle

connection makes the silica aerogel very brittle. Jiang et al. [183] mitigate this shortcoming by using natural cellulose prepared ink for printing a strong yet flexible structure. The cellulose ink underwent a shear-induced alignment during extrusion, along with the hydrogen-bonded crystalline microstructure, the 3D-printed cellulose

exhibits a ductile and superelastic mechanical property. Additionally, owing to the ultrahigh porosity (greater than 90%), the porous cellulose structure also demonstrates significant thermal insulation performance.

All the abovementioned works highlight that using additive manufacturing technologies, mesoporous building blocks can be shaped to highly customized 3D geometries. Moreover, the 3D printed models can well preserve the thermal insulation property/performance of the raw material feedstock.

#### 6.4. Tissue engineering

Recently, ink-based additive manufacturing has been largely involved in tissue engineering applications. This field requires highly customized and complex shapes that can mimic nature-inspired structures. However, traditional subtractive manufacturing has limitations in controlling the architecture as well as the microstructure. Taking advantage of biocompatible material feedstock, additive manufacturing techniques can construct it to functioning macroscopic pores and mimic the actual geometry such as bones and organs [152]. Furthermore, the unique freeform fabrication of AM can accurately 3D print the patient-specific geometries. DIW and SLA techniques are broadly used for creating the bionic structures with biocompatible materials, including Cellulose nanofibrils (CNF) [184,185], poly(ethylene glycol) diacrylate (PEGDA) [176], PEGDA/GelMA (gelatin methacrylate) [152], PEGDA/CNF [92], and Polycaprolactone (PCL) [186,187]. The biocompatibility of the 3D printed porous network was also examined. John et al. showed a 3D patterned multi-scale porous channels with nanofiber aerogels can significantly increase cell proliferation and migration on both the external and internal structures in vitro. Besides, more bold vessels can be formed across the multi-scale channels, indicating that it provides greater space for cell seeding. In contrast, the control group without the multi-scale channel can only seed limited cells at the surfaces, indicating a much lower cellular infiltration and neovascularization within the specimen.

Kang et al. [187] developed the ITOP (integrated tissue-organ printer) for ear cartilage reconstruction. Taking advantage of the multi-material printing capability of DIW, a multi-cartridge modulus was used to deposit different materials onto one specimen. An integrated multi-material structure realizes multiple functionalities. The biodegradable polymer (PCL) frame provides adequate structural support and resilience, and the porous composite hydrogel provides the microenvironment for cell proliferation. The fine 3D printed lattice pattern allows for improved nutrients and oxygen diffusion, which further promotes the cell viability in the printed porous structure. The printed specimen was implanted in mice for the in-vivo maturation test, and the results demonstrate that the printed ear-shape cartilage can function as those of native cartilage Table 4.

The hierarchical 3D porous structure of bone supports the structural integrity and provides the microenvironment and passageways for nutrients and oxygen. Specifically, the outer "compact bone" is less porous and closely packed, whereas the inner "spongy bone" is in highly interconnected open porous morphology. Conventional fabrication techniques such as freeze-casting, gas forming, and phase separation have intrinsic limitations for precise and consistent control of producing such porous structure [9]. Moreover, due to the vast complexity in bone structure across the population, the shape control is yet another challenge. Conversely, the additive manufacturing employs a wide variety of biocompatible materials, including hydroxyapatite (HAP) [104,135, 188], poly( $\epsilon$ -caprolactone) (PCL) [137], barium titanate (BaTiO<sub>3</sub>) [189] and can be printed to the scaffolds which mimic the actual geometry and properties of bones Figs. 11 and 12.

#### 7. Conclusion and perspectives

The combination of porous structure and additive manufacturing technologies not only realizes the fabrication of multi-scale porous

**Table 4**Application requirements of 3D printed porous structures.

Application		Preferable pore size	Preferable pore shape	Preferable pore morphology	Ref.
Adsorption	Pollutant removal	Submicron to nanoscale	Spherical shape	Open pore	[177]
	Water				[4,
	purification				190]
	Filtration				[91,
					191]
Insulation	Thermal insulation	Nanoscale	Stochastic pattern	Open pore	[55]
	Acoustic insulation	Micron-scale	Stochastic pattern	Closed pore	[192]
Bone repair		Hierarchical	Aligned	Closed pore	[134,
		multi-scale,	planar		193]
		from	shape		
		submicron to			
		micron-scale			
Mass transfer	/Nutrition	Micron-scale	Aligned	Open pore	[78,
transfer			planar		152]
			shape		
Energy storag	ge	Hierarchical	Spherical	Open pore	[28,
		multi-scale,	shape		194]
		from			
		submicron to			
F		micron-scale	A1:4	0	FO
Energy conve	rsion	Submicron-	Aligned	Open pore	[2,
		scale	planar shape		195]
Catalysis		Submicron-	snape Stochastic	Open pore	[139,
Catalysis		scale	pattern	Open pore	[139, 196]
Sensing		Micron-scale	Aligned	Open pore	[175]
Sensing		wiicioii-scale	planar shape	Open pore	[1/3]

networks in various sizes and shapes, but also improves the performance of the existing porous structures, which consequently promotes widespread emerging applications. Despite the significant advancement, many challenges and limitations need to be addressed in the following years. In this section, we discuss our perspectives on the major challenges in the field. Align with the bottom-up fashion of additive manufacturing, we begin the outlook discussion from the design of the porous structure, followed by materials and fabrication process, and eventually the property and performance.

#### 7.1. Perspectives and future outlooks: design

Nature provides exceptional guidance for designing highly optimized free structures. Most of the biological creatures have internal porous structures, which undergo evolutions that span centuries of time-scale. The nature-inspired structures have multi-scale, hierarchical, and optimally arranged porous networks, leading to multi-functionalities and enhanced performance. For applications in bone engineering and catalysts, the nature-inspired porous structures can effectively leverage the volume utilization and mass transfer. Moreover, 3D printing can produce the replicated nature-inspired structure, which largely shortens the production cycle compared to the long time-scale of natural evolution. However, only limited research has been carried out so far due to the many unknowns of the underlying mechanism of the biological evolutions. Modern artificial intelligence and machine learning are potentially powerful techniques for exploring nature-inspired multi-scale multi-functional porous structures.

On the other hand, engineered porous structures, such as the hierarchical metamaterial structure is an emerging porous network that can offer application-oriented properties. An engineered porous structure can be generated by periodically repeating the unit cell and finally forming a continuum solid material. The periodic pores can attain the targeted behavior by optimizing the underlying shape of the unit cells.

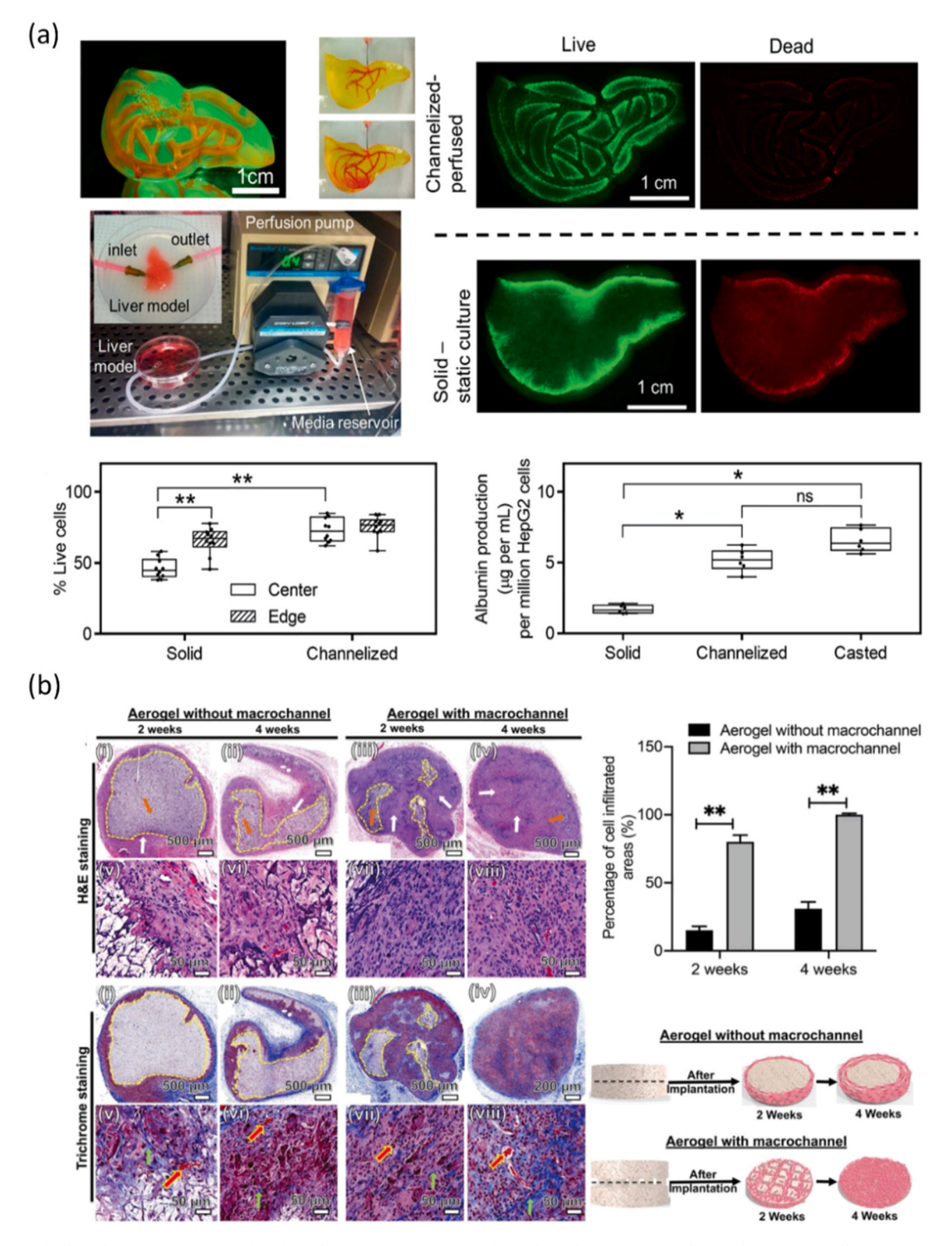


Fig. 11. Biomedical applications of 3D-printed multi-scale porous structure. (a) The multi-scale porous network provides an increased surface area, promoting nutrition transfer, which significantly increases cell viability. (b) Subcutaneous implantation of 3D PCL/gelatin biomimetic nanofiber aerogels with patterned macrochannels, providing an improved cellular infiltration and neovascularization.

(a) Reproduced with permission [152]. Copyright 2021, Wiley. (b) . Reproduced with permission [186]. Copyright 2021, Wiley.

Compared to the nature-inspired porous structure, the engineered porous structure is computationally achievable in the current stage. Besides, this strategy can also be utilized to create structures favorable for 3D printing process, avoiding the overhang structures, thus saving

the material consumption. However, 3D printing this type of architecture with high fidelity poses new challenges in ink design and tuning the rheological behavior.

To sum up, the design of multi-scale porous structures for additive

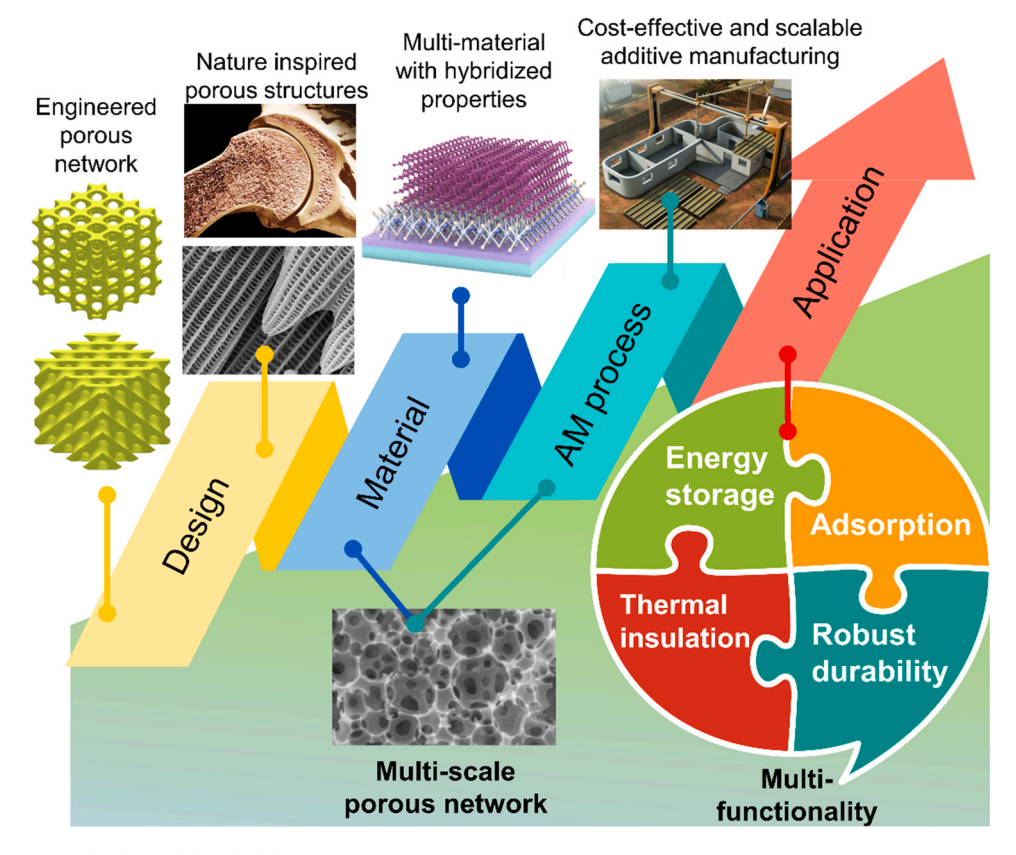


Fig. 12. Summary of future outlook of ink-based additive manufacturing for porous structures.

Schematic multi-material figure is reproduced with permission [199]. Copyright 2020, Springer Nature. (b) Microstructure of porous network is reproduced with permission [200]. Copyright 2015, Elsevier

manufacturing is still at the advent of AM technologies has led to great potential in the design of porous structures with unique and customized properties. The creation of nature-inspired design and the engineered porous structures are promising directions for future development.

# 7.2. Perspectives and future outlooks: materials and AM processes

Thus far, various AM technologies for porous structures have been explored, and their future development is an increasingly important pillar in the manufacturing field. However, transferring these cutting-edge technologies to manufacturing and scaling up the production remains a challenge. A scalable AM process with low cost and high efficiency for mid-volume or mass production is highly desired for the future. In this regard, the direct ink writing with ambient pressure drying process is a great fit to streamline scalable additive manufacturing. Evidenced by Sanandiya et al. [197] for DIW of wind turbine blades using cellulosic material and by the Khoshnevis group for DIW of houses [198]. However, the cost-effective DIW has inherent deficiencies in pore size control and arrangement. The potential solution may include optimizing the ink composition and linking the ink rheology behavior to the final property, such as the porosity and pore hierarchy.

On the other hand, a rapidly growing trend for future manufacturing systems is toward sustainable manufacturing. Sustainable practice in manufacturing would benefit the economy, environment, and future civilization. To this end, porous material manufacturing is facing significant challenges. As mentioned in the post-processing section (Section 4), the solvent exchanging process is the most effective method for creating the porous structure. Nevertheless, the enormous cost of energy consumption cannot be ignored. More importantly, the negative environmental impacts caused by irritants, even toxic solvents emissions, by no means are sustainable. In this sense, the DIW with ambient pressure

drying again finds a favorable spot since it has the least possible footprint to affect the environment negatively [7]. Material-wise, the current templating methods use a large amount of sacrificial and non-renewable materials, such as polymeric microbeads, which causes waste and even pollution during post-treatments. In this regard, freeze-drying with inkjet or DIW, where water is used as the templating material, is an efficient and sustainable way for porous fabrication.

From a technical perspective, with a better understanding of the merits and drawbacks of AM techniques, we could seamlessly interweave AM process and the conventional manufacturing approaches to develop strategies to fabricate multi-scale porous structures through the marriage of the merits from each technique. As introduced in Sections 3 and 4, the multi-scale porous networks can be 3D-printed via the multi-stage process, with various pore sizes, pore shapes, and precise controllability of porosity. Therefore, it requires great efforts and strides in multi-stage process design and optimization towards a higher level of combination and even synchronization.

Furthermore, with the multi-scale porous structures, exploring multimaterial printing is also a future direction. A mixture of multiple materials is widely observed in nature-inspired porous networks. The hybridized property of individual constituents leads to an impressive combination of mechanical, electrical, and other physical properties. In this sense, building the hybrid 3D printing process is essential for developing a hybrid ink deposition process. Each type of ink can be deposited using the most suitable process, offering more flexibility in ink formulation. For example, with a photocurable hydrogel material (e.g., PEGDA), SLA printing is the most suitable method for 3D shaping. On top of it, a sensing property can be achieved by embedding active material (e.g., PEDOT:PSS, graphene) within the hydrogel architecture, then inkjet printing could be used for depositing the active materials. The challenge of developing a hybrid process is how to synchronize the different types of AM processes. Sequentially depositing each ink should

be a good starting point. Another potential challenge is the binding between various materials in one specimen since different ink categories may require different post-processing methods. Taking use of chemical bonding could form better integrity. Functional groups such as carboxyl (COOH), amino (NH), amino (HN2), and ammonium (NH $_4$ <sup>+</sup>) are generic candidates for achieving chemical bonding.

#### 7.3. Perspectives and future outlooks: property and performance

As mentioned above, with future development on the nature-inspired multi-scale porous structure design, the multi-functionalities can be naturally achieved in the 3D printed porous network. For example, a combined functionality of robust mechanical property, hierarchical pore arrangement for mass transfer (in energy storage), or nutrition transfer (in bone and tissue) could be realized. As a matter of fact, even though it is demonstrated that 3D printed porous networks could significantly outperform their counterparts (e.g., energy storage, catalyst, water treatments), however, the ink is still not fully optimized for 3D printing. It's anticipated that with an optimized ink design and rheology behavior, the performance of 3D printed multi-scale porous network could be further improved. It also provides opportunities for promoting new applications such as triboelectric-based energy harvesting, solar energy storage, carbon dioxide capturing, oil refining, etc.

On the other hand, most of the current applications are still in the early stage, for example, the 3D printed batteries and bones are not fully compatible with long-term practical use. The in-depth research should be carried out to investigate long-term stability. For example, when using batteries in a harsh environment, their performance may get degraded over time. Then the studies on the mechanism of degradation and the side effects, particularly for the 3D printed multi-scale porous structures would demonstrate meaningful guidance. In turn, the findings may provide implications for optimizing the AM process.

In conclusion, the future development of additive manufacturing for porous structures requires intimate collaboration between different disciplines, including manufacturing, material science, chemistry, physics, biology, industrial and civil engineering. We dedicated this review to highlight the enormous advances of this field, and we also believe the environmental, economic, and social impacts of the 3D printed porous architectures will become increasingly significant in the future.

# **Declaration of Competing Interest**

The authors declare that they have no known competing financial interests or personal relationships that could have appeared to influence the work reported in this paper.

#### Acknowledgements

The authors would like to gratefully acknowledge the support from U.S. National Science Foundation, USA, (NSF), through the award CMMI-1846863, and the U.S. Department of Energy, Office of Energy Efficiency and Renewable Energy, USA, through grant DEEE-0008675.

# References

- [1] F. Hu, S. Wu, Y. Sun, Hollow-structured materials for thermal insulation, Adv. Mater. 31 (38) (2019), 1801001, https://doi.org/10.1002/adma.201801001.
- [2] M.-H. Sun, S.-Z. Huang, L.-H. Chen, Y. Li, X.-Y. Yang, Z.-Y. Yuan, B.-L. Su, Applications of hierarchically structured porous materials from energy storage and conversion, catalysis, photocatalysis, adsorption, separation, and sensing to biomedicine. Chem. Soc. Rev. 45 (12) (2016) 3479–3563.
- [3] K.Y. Morgan, D. Sklaviadis, Z.L. Tochka, K.M. Fischer, K. Hearon, T.D. Morgan, R. Langer, L.E. Freed, Multi-material tissue engineering scaffold with hierarchical pore architecture, Adv. Funct. Mater. 26 (32) (2016) 5873–5883, https://doi. org/10.1002/adfm.201601146.
- [4] A. Masud, C. Zhou, N. Aich, Emerging investigator series: 3D printed graphene-biopolymer aerogels for water contaminant removal: a proof of concept, Environ. Sci. Nano 8 (2020) 399–414, https://doi.org/10.1039/D0EN00953A.

- [5] D. Zeng, J. Wu, J.F. Kennedy, Application of a chitosan flocculant to water treatment, Carbohydr. Polym. 71 (1) (2008) 135–139.
- [6] V. Middelkoop, T. Slater, M. Florea, F. Neaţu, S. Danaci, V. Onyenkeadi, K. Boonen, B. Saha, I.-A. Baragau, S. Kellici, Next frontiers in cleaner synthesis: 3D printed graphene-supported CeZrLa mixed-oxide nanocatalyst for CO<sub>2</sub> utilisation and direct propylene carbonate production, J. Clean. Prod. 214 (2019) 606–614, https://doi.org/10.1016/j.jclepro.2018.12.274.
- [7] Z. Guo, R. Yang, T. Wang, L. An, S. Ren, C. Zhou, Cost-effective additive manufacturing of ambient pressure-dried silica aerogel, J. Manuf. Sci. Eng. 143 (2021) 1.
- [8] M. Rethinasabapathy, S.-M. Kang, S.-C. Jang, Y.S. Huh, Three-dimensional porous graphene materials for environmental applications, Carbon Lett. 22 (2017) 1–13.
- [9] S.H. Jariwala, G.S. Lewis, Z.J. Bushman, J.H. Adair, H.J. Donahue, 3D printing of personalized artificial bone scaffolds, 3D Print. Addit. Manuf. 2 (2) (2015) 56–64, https://doi.org/10.1089/3dp.2015.0001.
- [10] T. Godefroidt, N. Ooms, B. Pareyt, K. Brijs, J.A. Delcour, Ingredient functionality during foam-type cake making: a review, Compr. Rev. Food Sci. Food Saf. 18 (5) (2019) 1550–1562, https://doi.org/10.1111/1541-4337.12488.
- [11] A.R. Studart, U.T. Gonzenbach, E. Tervoort, L.J. Gauckler, Processing routes to macroporous ceramics: a review, J. Am. Ceram. Soc. 89 (6) (2006) 1771–1789, https://doi.org/10.1111/j.1551-2916.2006.01044.x.
- 12 F. Matter, A.L. Luna, M. Niederberger, From colloidal dispersions to aerogels: How to master nanoparticle gelation, Nano Today 30 (2020), 100827, https://doi.org/ 10.1016/i.nantod.2019.100827.
- [13] P. Patil, S. Patil, P. Kate, A.A. Kulkarni, Inkjet printing of silver nanowires on flexible surfaces and methodologies to improve the conductivity and stability of the printed patterns, Nanoscale Adv. 3 (1) (2021) 240–248, https://doi.org/ 10.1039/D0NA00684J.
- [14] D.J. Finn, M. Lotya, J.N. Coleman, Inkjet printing of silver nanowire networks, ACS Appl. Mater. Interfaces 7 (17) (2015) 9254–9261, https://doi.org/10.1021/ acsami.5b01875.
- [15] B. Chen, S.R. Das, W. Zheng, B. Zhu, B. Xu, S. Hong, C. Sun, X. Wang, Y. Wu, J. C. Claussen, Inkjet printing of single-crystalline Bi2Te3 thermoelectric nanowire networks, Adv. Electron. Mater. 3 (4) (2017), 1600524, https://doi.org/10.1002/aelm.201600524.
- [16] K.-H. Choi, J. Yoo, C.K. Lee, S.-Y. Lee, All-inkjet-printed, solid-state flexible supercapacitors on paper, Energy Environ. Sci. 9 (9) (2016) 2812–2821, https://doi.org/10.1039/C6EE00966B.
- [17] E. Brown, P. Yan, H. Tekik, A. Elangovan, J. Wang, D. Lin, J. Li, 3D printing of hybrid MoS2-graphene aerogels as highly porous electrode materials for sodium ion battery anodes, Mater. Des. 170 (2019), 107689.
- 18 Q. Zhang, F. Zhang, S.P. Medarametla, H. Li, C. Zhou, D. Lin, 3D printing of graphene aerogels, Small 12 (13) (2016) 1702–1708.
- [19] S. Kommeren, M.J. Coenen, T.M. Eggenhuisen, T.W. Slaats, H. Gorter, P. Groen, Combining solvents and surfactants for inkjet printing PEDOT: PSS on P3HT/ PCBM in organic solar cells, Org. Electron. 61 (2018) 282–288.
- [20] J. Vaithilingam, E. Saleh, L. Körner, R.D. Wildman, R.J. Hague, R.K. Leach, C. J. Tuck, 3-dimensional inkjet printing of macro structures from silver nanoparticles. Mater. Des. 139 (2018) 81–88.
- [21] Z. Chen, N. Brandon, Inkjet printing and nanoindentation of porous alumina multilayers, Ceram. Int. 42 (7) (2016) 8316–8324, https://doi.org/10.1016/j ceramint.2016.02.045.
- [22] B.W. An, K. Kim, H. Lee, S.Y. Kim, Y. Shim, D.Y. Lee, J.Y. Song, J.U. Park, High-resolution printing of 3D structures using an electrohydrodynamic inkjet with multiple functional inks, Adv. Mater. 27 (29) (2015) 4322–4328, https://doi.org/10.1002/adma.201502092.
- [23] M. Arin, P. Lommens, N. Avci, S.C. Hopkins, K. De Buysser, I.M. Arabatzis, I. Fasaki, D. Poelman, I. Van Driessche, Inkjet printing of photocatalytically active TiO2 thin films from water based precursor solutions, J. Eur. Ceram. Soc. 31 (6) (2011) 1067–1074
- [24] T. Li, Y. Dong, D. Yuan, Y. Liu, Modification of inkjet printer for polymer sensitive layer preparation on silicon-based gas sensors, AIP Adv. 5 (4) (2015), 041327, https://doi.org/10.1063/1.4914937.
- [25] N.O. Muniz, F.A. Vechietti, L.A.L. dos Santos, Influence of several binders on the mechanical properties of alumina parts manufactured by 3D inkjet printing, Mater. Res. Express 6 (11) (2019), 115341.
- [26] J.A. Lewis, J.E. Smay, J. Stuecker, J. Cesarano, Direct ink writing of three-dimensional ceramic structures. J. Am. Ceram. Soc. 89 (12) (2006) 3599–3609, https://doi.org/10.1111/ji.1551-2916.2006.01382.x.
- [27] J.A. Lewis, G.M. Gratson, Direct writing in three dimensions, Mater. Today 7 (7–8) (2004) 32–39, https://doi.org/10.1016/S1369-7021(04)00344-X.
- 28 F. Zhang, M. Wei, V.V. Viswanathan, B. Swart, Y. Shao, G. Wu, C. Zhou, 3D printing technologies for electrochemical energy storage, Nano Energy 40 (2017) 418–431.
- [29] F. Zhang, F. Yang, D. Lin, C. Zhou, Parameter study of three-dimensional printing graphene oxide based on directional freezing, J. Manuf. Sci. Eng. 139 (3) (2016) 031016, https://doi.org/10.1115/1.4034669.
- [30] G. Zhao, C. Zhou, D. Lin, Tool path planning for directional freezing-based threedimensional printing of nanomaterials, J. Micro Nano-Manuf. 6 (1) (2017), https://doi.org/10.1115/1.4038452.
- [31] F. Lübkemann, J.F. Miethe, F. Steinbach, P. Rusch, A. Schlosser, D. Zámbó, T. Heinemeyer, D. Natke, D. Zok, D. Dorfs, Patterning of nanoparticle-based aerogels and xerogels by inkjet printing, Small 15 (39) (2019), 1902186, https://doi.org/10.1002/smll.201902186
- [32] L. Liu, X. Wang, A. Lennon, B. Hoex, Geometric confinement of directly deposited features on hydrophilic rough surfaces using a sacrificial layer, J. Mater. Sci. 49 (12) (2014) 4363–4370, https://doi.org/10.1007/s10853-014-8135-1.

- [33] S. Schiaffino, A.A. Sonin, Molten droplet deposition and solidification at low Weber numbers, Phys. Fluids 9 (11) (1997) 3172–3187, https://doi.org/ 10.1063/1.869434.
- [34] K.A. Seerden, N. Reis, J.R. Evans, P.S. Grant, J.W. Halloran, B. Derby, Ink-jet printing of wax-based alumina suspensions, J. Am. Ceram. Soc. 84 (11) (2001) 2514–2520, https://doi.org/10.1111/j.1151-2916.2001.tb01045.x.
- 35 Kim, D., J.H. Yoo, Y. Lee, W. Choi, K. Yoo, J.-B. Lee. Gallium-based liquid metal inkjet printing. In Proceeding of the 2014 IEEE 27th International Conference on Micro Electro Mechanical Systems (MEMS). 2014. IEEE DOI: 10.1109/ MEMSYS.2014.6765804.
- [36] T.R. Lear, S.-H. Hyun, J.W. Boley, E.L. White, D.H. Thompson, R.K. Kramer, Liquid metal particle popping: Macroscale to nanoscale, Extrem. Mech. Lett. 13 (2017) 126–134, https://doi.org/10.1016/j.eml.2017.02.009.
- [37] Q. Cheng, Y. Liu, J. Lyu, Q. Lu, X. Zhang, W. Song, 3D printing-directed auxetic Kevlar aerogel architectures with multiple functionalization options, J. Mater. Chem. A 8 (28) (2020) 14243–14253, https://doi.org/10.1039/D0TA02590A.
- 38 E.A. Roth, T. Xu, M. Das, C. Gregory, J.J. Hickman, T. Boland, Inkjet printing for high-throughput cell patterning, Biomaterials 25 (17) (2004) 3707–3715, https:// doi.org/10.1016/j.biomaterials.2003.10.052.
- [39] N. Nekrasov, A. Emelianov, D. Kireev, N. Omerović, I. Bobrinetskiy, Photosensitive junctions based on UV-modified graphene and inkjet-printed organic molecules, Int. Soc. Opt. Photonics (2020), https://doi.org/10.1117/ 12.2560646.
- [40] Y. Yuan, Y. Zhang, R. Liu, J. Liu, Z. Li, X. Liu, Humidity sensor fabricated by inkjet-printing photosensitive conductive inks PEDOT: PVMA on a paper substrate, RSC Adv. 6 (53) (2016) 47498–47508, https://doi.org/10.1039/ C6RA03050E.
- [41] F. Tricot, F. Vocanson, D. Chaussy, D. Beneventi, Y. Lefkir, N. Destouches, Photosensitive ink formulation and inkjet printing on flexible PET substrate, J. Coat. Technol. Res. 16 (1) (2019) 113–123.
- [42] S.Q. Arlington, S.C. Barron, J.B. DeLisio, J.C. Rodriguez, S. Vummidi Lakshman, T.P. Weihs, G.M. Fritz, Multifunctional reactive nanocomposites via direct ink writing, Adv. Mater. Technol. 6 (5) (2021), 2001115, https://doi.org/10.1002/ admt.202001115.
- [43] A. Nommeots-Nomm, P.D. Lee, J.R. Jones, Direct ink writing of highly bioactive glasses, J. Eur. Ceram. Soc. 38 (3) (2018) 837–844, https://doi.org/10.1016/j. jeurceramsoc.2017.08.006.
- [44] J. Liao, H. Chen, H. Luo, X. Wang, K. Zhou, D. Zhang, Direct ink writing of zirconia three-dimensional structures, J. Mater. Chem. C 5 (24) (2017) 5867–5871, https://doi.org/10.1039/C7TC01545C.
- [45] B.-y Ye, C.-k Song, H. Huang, Q.-b Li, C.-w An, J.-y Wang, Direct ink writing of 3D-honeycombed CL-20 structures with low critical size, Def. Technol. 16 (3) (2020) 588–595, https://doi.org/10.1016/j.dt.2019.08.019.
- [46] J.W. Kemp, N.S. Hmeidat, B.G. Compton, Boron nitride-reinforced polysilazane-derived ceramic composites via direct-ink writing, J. Am. Ceram. Soc. 103 (8) (2020) 4043–4050, https://doi.org/10.1111/jace.17084.
- [47] N.S. Hmeidat, R.C. Pack, S.J. Talley, R.B. Moore, B.G. Compton, Mechanical anisotropy in polymer composites produced by material extrusion additive manufacturing, Addit. Manuf. 34 (2020), 101385.
- [48] L. Jiang, M. Rahnama, B. Zhang, X. Zhu, P.-C. Sui, D.-D. Ye, N. Djilali, Predicting the interaction between nanoparticles in shear flow using lattice Boltzmann method and Derjaguin–Landau–Verwey–Overbeek (DLVO) theory, Phys. Fluids 32 (4) (2020), 043302, https://doi.org/10.1063/1.5142669.
- 49 I. Szleifer, R. Yerushalmi-Rozen, Polymers and carbon nanotubes—dimensionality, interactions and nanotechnology, Polymer 46 (19) (2005) 7803–7818, https://doi.org/10.1016/j.polymer.2005.05.104.
- 50 S.W. Charles, J. Popplewell, Properties and applications of magnetic liquids, Endeavour 6 (4) (1982) 153–161.
- [51] F. Li, D.P. Josephson, A. Stein, Colloidal assembly: the road from particles to colloidal molecules and crystals, Angew. Chem. Int. Ed. 50 (2) (2011) 360–388, https://doi.org/10.1002/anie.201001451.
- [52] H. Zhou, X. Wang, X. Wang, C. Peng, R. Wang, K. Zhou, Principles of dispersing powders for 3D printing, Colloids Interfaces 5 (2) (2021) 25, https://doi.org/ 10.3390/colloids5020025.
- [53] B. Vincent, Early (pre-DLVO) studies of particle aggregation, Adv. Colloid Interface Sci. 170 (1–2) (2012) 56–67, https://doi.org/10.1016/j. cis.2011.12.003.
- 54 M.E. Leunissen, C.G. Christova, A.-P. Hynninen, C.P. Royall, A.I. Campbell, A. Imhof, M. Dijkstra, R. Van Roij, A. Van Blaaderen, Ionic colloidal crystals of oppositely charged particles, Nature 437 (7056) (2005) 235–240, https://doi.org/ 10.1038/nature03946.
- 55 S. Zhao, G. Siqueira, S. Drdova, D. Norris, C. Ubert, A. Bonnin, S. Galmarini, M. Ganobjak, Z. Pan, S. Brunner, Additive manufacturing of silica aerogels, Nature 584 (7821) (2020) 387–392, https://doi.org/10.1038/s41586-020-2594-0.
- [56] B.A. Dikici, F. Claeyssens, Basic principles of emulsion templating and its use as an emerging manufacturing method of tissue engineering scaffolds, Front. Bioeng. Biotechnol. 8 (2020), https://doi.org/10.3389/fbioe.2020.00875.
- [57] M.A. Torres Arango, D. Kwakye-Ackah, S. Agarwal, R.K. Gupta, K.A. Sierros, Environmentally friendly engineering and three-dimensional printing of TiO2 hierarchical mesoporous cellular architectures, ACS Sustain. Chem. Eng. 5 (11) (2017) 10421–10429, https://doi.org/10.1021/acssuschemeng.7b02450.
- [58] S.S. Chan, M.L. Sesso, G.V. Franks, Direct ink writing of hierarchical porous alumina-stabilized emulsions: rheology and printability, J. Am. Ceram. Soc. 103 (10) (2020) 5554–5566.

- [59] L. Alison, S. Menasce, F. Bouville, E. Tervoort, I. Mattich, A. Ofner, A.R. Studart, 3D printing of sacrificial templates into hierarchical porous materials, Sci. Rep. 9 (1) (2019) 1–9, https://doi.org/10.1038/s41598-018-36789-z.
- [60] Y. Hu, J. Wang, X. Li, X. Hu, W. Zhou, X. Dong, C. Wang, Z. Yang, B.P. Binks, Facile preparation of bioactive nanoparticle/poly (ε-caprolactone) hierarchical porous scaffolds via 3D printing of high internal phase Pickering emulsions, J. Colloid Interface Sci. 545 (2019) 104–115, https://doi.org/10.1016/j. icis.2019.03.024.
- [61] C. Minas, D. Carnelli, E. Tervoort, A.R. Studart, 3D printing of emulsions and foams into hierarchical porous ceramics, Adv. Mater. 28 (45) (2016) 9993–9999, https://doi.org/10.1002/adma.201603390.
- [62] I. Cooperstein, M. Layani, S. Magdassi, 3D printing of porous structures by UV-curable O/W emulsion for fabrication of conductive objects, J. Mater. Chem. C 3 (9) (2015) 2040–2044.
- [63] J.T. Muth, P.G. Dixon, L. Woish, L.J. Gibson, J.A. Lewis, Architected cellular ceramics with tailored stiffness via direct foam writing, Proc. Natl. Acad. Sci. 114 (8) (2017) 1832–1837, https://doi.org/10.1073/pnas.1616769114.
- [64] Z. Guo, L. An, S. Lakshmanan, J. Armstrong, S. Ren, C. Zhou, Additive manufacturing of porous ceramics with foaming agent, J. Manuf. Sci. Eng. (2021) 1–21, https://doi.org/10.1115/1.4051828.
- [65] K. Huang, H. Elsayed, G. Franchin, P. Colombo, 3D printing of polymer-derived SiOC with hierarchical and tunable porosity, Addit. Manuf. 36 (2020), 101549, https://doi.org/10.1016/j.addma.2020.101549.
- [66] P. Colombo, E. Bernardo, L. Biasetto, Novel microcellular ceramics from a silicone resin, J. Am. Ceram. Soc. 87 (1) (2004) 152–154.
- [67] H. Jin, Z. Yang, H. Li, D. Jia, Y. Zhou, Fabrication of Si2N2O ceramic foam by combination of direct ink writing and biological foaming techniques, Adv. Eng. Mater. 22 (4) (2020), 1901541.
- [68] L. Zhang, F. Zhang, Y. Wang, R. Han, J. Chen, R. Zhang, E. Chu, In-situ preparation of copper azide by direct ink writing, Mater. Lett. 238 (2019) 130–133, https://doi.org/10.1016/j.matlet.2018.11.165.
- 69 T. Uchida, H. Onoe, 4D printing of multi-hydrogels using direct ink writing in a supporting viscous liquid, Micromachines 10 (7) (2019) 433, https://doi.org/ 10.3390/mi10070433.
- [70] S. Tagliaferri, A. Panagiotopoulos, C. Mattevi, Direct ink writing of energy materials, Mater. Adv. 2 (2020) 540–563, https://doi.org/10.1039/ D0MA00753F.
- 71 G.M. Gratson, M. Xu, J.A. Lewis, Direct writing of three-dimensional webs, nature 428 (6981) (2004) 386, 386-386.
- [72] N.W.S. Pinargote, A. Smirnov, N. Peretyagin, A. Seleznev, P. Peretyagin, Direct ink writing technology (3D printing) of graphene-based ceramic nanocomposites: a review, Nanomaterials 10 (7) (2020) 1300, https://doi.org/10.3390/ nano10071300.
- [73] C. Zhu, T. Liu, F. Qian, T.Y.-J. Han, E.B. Duoss, J.D. Kuntz, C.M. Spadaccini, M. A. Worsley, Y. Li, Supercapacitors based on three-dimensional hierarchical graphene aerogels with periodic macropores, Nano Lett. 16 (6) (2016) 3448–3456, https://doi.org/10.1021/acs.nanolett.5b04965.
- [74] C. Zhu, T.Y.-J. Han, E.B. Duoss, A.M. Golobic, J.D. Kuntz, C.M. Spadaccini, M. A. Worsley, Highly compressible 3D periodic graphene aerogel microlattices, Nat. Commun. 6 (1) (2015) 1–8.
- [75] Y.-W. Moon, I.-J. Choi, Y.-H. Koh, H.-E. Kim, Porous alumina ceramic scaffolds with biomimetic macro/micro-porous structure using three-dimensional (3-D) ceramic/camphene-based extrusion, Ceram. Int. 41 (9) (2015) 12371–12377.
- [76] W. Zhang, I. Ullah, L. Shi, Y. Zhang, H. Ou, J. Zhou, M.W. Ullah, X. Zhang, W. Li, Fabrication and characterization of porous polycaprolactone scaffold via extrusion-based cryogenic 3D printing for tissue engineering, Mater. Des. 180 (2019), 107946.
- 77 C. Liu, X. Cheng, B. Li, Z. Chen, S. Mi, C. Lao, Fabrication and characterization of 3D-printed highly-porous 3D LiFePO4 electrodes by low temperature direct writing process, Materials 10 (8) (2017) 934.
- [78] L. Chen, X. Tang, P. Xie, J. Xu, Z. Chen, Z. Cai, P. He, H. Zhou, D. Zhang, T. Fan, 3D printing of artificial leaf with tunable hierarchical porosity for CO<sub>2</sub> photoreduction, Chem. Mater. 30 (3) (2018) 799–806, https://doi.org/10.1021/acs.chemmater.7b04313.
- [79] X. Song, Y. Chen, T.W. Lee, S. Wu, L. Cheng, Ceramic fabrication using maskimage-projection-based stereolithography integrated with tape-casting, J. Manuf. Process. 20 (2015) 456–464.
- 80 L. He, X. Song, Supportability of a high-yield-stress slurry in a new stereolithography-based ceramic fabrication process, Jom 70 (3) (2018) 407–412.
- [81] L. He, F. Fei, W. Wang, X. Song, Support-free ceramic stereolithography of complex overhanging structures based on an elasto-viscoplastic suspension feedstock, ACS Appl. Mater. Interfaces 11 (20) (2019) 18849–18857.
- [82] Q. Lian, W. Sui, X. Wu, F. Yang, S. Yang, Additive manufacturing of ZrO2 ceramic dental bridges by stereolithography, Rapid Prototyp. J. 24 (2018) 114–119.
- [83] W. Bian, D. Li, Q. Lian, X. Li, W. Zhang, K. Wang, Z. Jin, Fabrication of a bioinspired beta-Tricalcium phosphate/collagen scaffold based on ceramic stereolithography and gel casting for osteochondral tissue engineering, Rapid Prototyp. J. 18 (2012) 68–80, https://doi.org/10.1108/13552541211193511.
- [84] T. Aubert, J.-Y. Huang, K. Ma, T. Hanrath, U. Wiesner, Porous cage-derived nanomaterial inks for direct and internal three-dimensional printing, Nat. Commun. 11 (1) (2020) 1–9.
- [85] X. Song, Z. Zhang, Z. Chen, Y. Chen, Porous structure fabrication using a stereolithography-based sugar foaming method, J. Manuf. Sci. Eng. 139 (3) (2017) 031015.

- [86] X. Mu, T. Bertron, C. Dunn, H. Qiao, J. Wu, Z. Zhao, C. Saldana, H. Qi, Porous polymeric materials by 3D printing of photocurable resin, Mater. Horiz. 4 (3) (2017) 442–449, https://doi.org/10.1039/C7MH00084G.
- [87] S. Saeed, R.M. Al-Sobaihi, M.F. Bertino, L.S. White, K.M. Saoud, Laser induced instantaneous gelation: aerogels for 3D printing, J. Mater. Chem. A 3 (34) (2015) 17606–17611, https://doi.org/10.1039/c5ta04215.
- [88] K.M. Saoud, S. Saeed, M.F. Bertino, L.S. White, Fabrication of strong and ultralightweight silica-based aerogel materials with tailored properties, J. Porous Mater. 25 (2) (2018) 511–520, https://doi.org/10.1007/s10934-017-0463-5.
- [89] I. Cooperstein, E. Shukrun, O. Press, A. Kamyshny, S. Magdassi, Additive manufacturing of transparent silica glass from solutions, ACS Appl. Mater. Interfaces 10 (22) (2018) 18879–18885.
- [90] Y. Hu, S. Broderick, Z. Guo, A.T. N'Diaye, J.S. Bola, H. Malissa, C. Li, Q. Zhang, Y. Huang, Q. Jia, Proton switching molecular magnetoelectricity, Nat. Commun. 12 (1) (2021) 1–9, https://doi.org/10.1038/s41467-021-24941-9.
- [91] Z. Dong, H. Cui, H. Zhang, F. Wang, X. Zhan, F. Mayer, B. Nestler, M. Wegener, P. A. Levkin, 3D printing of inherently nanoporous polymers via polymerization-induced phase separation, Nat. Commun. 12 (1) (2021) 1–12, https://doi.org/10.1038/s41467-020-20498-1.
- [92] D. Sun, W. Liu, A. Tang, F. Guo, W. Xie, A new PEGDA/CNF aerogel-wet hydrogel scaffold fabricated by a two-step method, Soft Matter 15 (40) (2019) 8092–8101, https://doi.org/10.1039/c9sm00899c.
- 93 D. Jang, D. Kim, J. Moon, Influence of fluid physical properties on ink-jet printability, Langmuir 25 (5) (2009) 2629–2635.
- [94] L.J. Segura, T. Wang, C. Zhou, H. Sun, Online droplet anomaly detection from streaming videos in inkjet printing, Addit. Manuf. 38 (2021), 101835.
- [95] X. Wang, W.W. Carr, D.G. Bucknall, J.F. Morris, High-shear-rate capillary viscometer for inkjet inks, Rev. Sci. Instrum. 81 (6) (2010), 065106, https://doi. org/10.1063/1.3449478
- [96] X. Wang, W.W. Carr, D.G. Bucknall, J.F. Morris, Drop-on-demand drop formation of colloidal suspensions, Int. J. Multiph. Flow. 38 (1) (2012) 17–26, https://doi. org/10.1016/j.ijmultiphaseflow.2011.09.001.
- [97] L.J. Segura, G. Zhao, C. Zhou, H. Sun, Nearest neighbor gaussian process emulation for multi-dimensional array responses in freeze nano 3D printing of energy devices, J. Comput. Inf. Sci. Eng. 20 (4) (2020), https://doi.org/10.1115/ 1.4045795.
- [98] J. Huang, L.J. Segura, T. Wang, G. Zhao, H. Sun, C. Zhou, Unsupervised learning for the droplet evolution prediction and process dynamics understanding in inkjet printing, Addit. Manuf. 35 (2020), 101197.
- [99] T. Wang, T.-H. Kwok, C. Zhou, S. Vader, In-situ droplet inspection and closed-loop control system using machine learning for liquid metal jet printing, J. Manuf. Syst. 47 (2018) 83–92.
- [100] D. Cao, Y. Xing, K. Tantratian, X. Wang, Y. Ma, A. Mukhopadhyay, Z. Cheng, Q. Zhang, Y. Jiao, L. Chen, 3D printed high-performance lithium metal microbatteries enabled by nanocellulose. Adv. Mater. 31 (14) (2019), 1807313.
- [101] J. Feng, B.-L. Su, H. Xia, S. Zhao, C. Gao, L. Wang, O. Ogbeide, J. Feng, T. Hasan, Printed aerogels: chemistry, processing, and applications, Chem. Soc. Rev. 50 (2021) 3842–3888, https://doi.org/10.1039/C9CS00757A.
- [102] B. Derby, Inkjet printing ceramics: from drops to solid, J. Eur. Ceram. Soc. 31 (14) (2011) 2543–2550, https://doi.org/10.1016/j.jeurceramsoc.2011.01.016.
- [103] Y. Hu, Z. Guo, A. Ragonese, T. Zhu, S. Khuje, C. Li, J.C. Grossman, C. Zhou, M. Nouh, S. Ren, A 3D-printed molecular ferroelectric metamaterial, Proc. Natl. Acad. Sci. 117 (44) (2020) 27204–27210.
- [104] Z. Wang, C. Huang, J. Wang, B. Zou, Development of a novel aqueous hydroxyapatite suspension for stereolithography applied to bone tissue engineering, Ceram. Int. 45 (3) (2019) 3902–3909.
- [105] W.-D. Li, C. Wang, Z.-H. Jiang, L.-J. Chen, Y.-H. Wei, L.-Y. Zhang, M.-Y. Chen, X. Yang, G.-J. Zhang, Stereolithography based additive manufacturing of high-k polymer matrix composites facilitated by thermal plasma processed barium titanate microspheres, Mater. Des. 192 (2020), 108733.
- [106] S.H. Kim, Y.K. Yeon, J.M. Lee, J.R. Chao, Y.J. Lee, Y.B. Seo, M.T. Sultan, O.J. Lee, J.S. Lee, S.-I. Yoon, Precisely printable and biocompatible silk fibroin bioink for digital light processing 3D printing, Nat. Commun. 9 (1) (2018) 1–14.
- [107] K. Zhang, C. Xie, G. Wang, R. He, G. Ding, M. Wang, D. Dai, D. Fang, High solid loading, low viscosity photosensitive Al2O3 slurry for stereolithography based additive manufacturing, Ceram. Int. 45 (1) (2019) 203–208, https://doi.org/ 10.1016/j.ceramint.2018.09.152.
- [108] T. Sekitani, H. Nakajima, H. Maeda, T. Fukushima, T. Aida, K. Hata, T. Someya, Stretchable active-matrix organic light-emitting diode display using printable elastic conductors, Nat. Mater. 8 (6) (2009) 494–499.
- [109] M. Su, F. Li, S. Chen, Z. Huang, M. Qin, W. Li, X. Zhang, Y. Song, Nanoparticle based curve arrays for multirecognition flexible electronics, Adv. Mater. 28 (7) (2016) 1369–1374, https://doi.org/10.1002/adma.201504759.
- 110 S. Lee, Y. Lee, J. Park, D. Choi, Stitchable organic photovoltaic cells with textile electrodes, Nano Energy 9 (2014) 88–93.
- [111] Y. Sun, Y. Zhang, Q. Liang, Y. Zhang, H. Chi, Y. Shi, D. Fang, Solvent inkjet printing process for the fabrication of polymer solar cells, RSC Adv. 3 (30) (2013) 11925–11934, https://doi.org/10.1039/C3RA22659J.
- [112] E. Katzir, S. Yochelis, Y. Paltiel, S. Azoubel, A. Shimoni, S. Magdassi, Tunable inkjet printed hybrid carbon nanotubes/nanocrystals light sensor, Sens. Actuators B Chem. 196 (2014) 112–116.
- 113 S. Ali, A. Hassan, G. Hassan, J. Bae, C.H. Lee, All-printed humidity sensor based on graphene/methyl-red composite with high sensitivity, Carbon 105 (2016) 23–32.
- [114] C. Yang, A. Abodurexiti, X. Maimaitiyiming, Flexible humidity and pressure sensors realized by molding and inkjet printing processes with sandwich structure, Macromol. Mater. Eng. 305 (8) (2020), 2000287.

- [115] G. Zhao, C. Zhou, D. Lin, Tool path planning for directional freezing-based threedimensional printing of nanomaterials, J. Micro Nano-Manuf. 6 (2018) 1.
- [116] H. Tetik, G. Yang, W. Tan, A. Fong, S. Lei, J.N. Weker, D. Lin, High speed in-situ X-ray imaging of 3D freeze printing of aerogels, Addit. Manuf. 36 (2020), 101513.
- 117 P. Yan, E. Brown, Q. Su, J. Li, J. Wang, C. Xu, C. Zhou, D. Lin, 3D printing hierarchical silver nanowire aerogel with highly compressive resilience and tensile elongation through tunable poisson's ratio, Small 13 (38) (2017), 1701756, https://doi.org/10.1002/smll.201701756.
- [118] Q. Zhang, D. Lin, B. Deng, X. Xu, Q. Nian, S. Jin, K.D. Leedy, H. Li, G.J. Cheng, Flyweight, superelastic, electrically conductive, and flame-retardant 3D multinanolayer graphene/ceramic metamaterial, Adv. Mater. 29 (28) (2017), 1605506, https://doi.org/10.1126/science.aav730.
- [119] M. Dankoco, G. Tesfay, E. Bènevent, M. Bendahan, Temperature sensor realized by inkjet printing process on flexible substrate, Mater. Sci. Eng. B 205 (2016) 1–5.
- [120] P.Q. Nguyen, L.-P. Yeo, B.-K. Lok, Y.-C. Lam, Patterned surface with controllable wettability for inkjet printing of flexible printed electronics, ACS Appl. Mater. Interfaces 6 (6) (2014) 4011–4016.
- [121] L. Dong, Z. Chen, X. Zhao, J. Ma, S. Lin, M. Li, Y. Bao, L. Chu, K. Leng, H. Lu, A non-dispersion strategy for large-scale production of ultra-high concentration graphene slurries in water, Nat. Commun. 9 (1) (2018) 1–8, https://doi.org/ 10.1038/s41467-017-02580-3.
- [122] T. Ma, P.R. Chang, P. Zheng, F. Zhao, X. Ma, Fabrication of ultra-light graphene-based gels and their adsorption of methylene blue, Chem. Eng. J. 240 (2014) 595–600.
- [123] H. Tetik, K. Zhao, N. Shah, D. Lin, 3D freeze-printed cellulose-based aerogels: obtaining truly 3D shapes, and functionalization with cross-linking and conductive additives, J. Manuf. Process. 68 (2021) 445–453, https://doi.org/ 10.1016/j.jmapro.2021.05.051.
- [124] J.M. Ortega, M. Golobic, J.D. Sain, J.M. Lenhardt, A.S. Wu, S.E. Fisher, L.X. Perez Perez, A.W. Jaycox, J.E. Smay, E.B. Duoss, Active mixing of disparate inks for multimaterial 3D printing, Adv. Mater. Technol. 4 (7) (2019), 1800717.
- [125] C. Bai, G. Franchin, H. Elsayed, A. Zaggia, L. Conte, H. Li, P. Colombo, High-porosity geopolymer foams with tailored porosity for thermal insulation and wastewater treatment, J. Mater. Res. 32 (17) (2017) 3251–3259, https://doi.org/10.1557/jmr.2017.127.
- [126] P. He, X. Tang, L. Chen, P. Xie, L. He, H. Zhou, D. Zhang, T. Fan, Patterned carbon nitride-based hybrid aerogel membranes via 3D printing for broadband solar wastewater remediation, Adv. Funct. Mater. 28 (29) (2018), 1801121, https:// doi.org/10.1002/adfm.201801121.
- [127] T. Nathan-Walleser, I.M. Lazar, M. Fabritius, F.J. Tölle, Q. Xia, B. Bruchmann, S. S. Venkataraman, M.G. Schwab, R. Mülhaupt, 3D Micro-extrusion of graphene-based active electrodes: towards high-rate AC line filtering performance electrochemical capacitors, Adv. Funct. Mater. 24 (29) (2014) 4706–4716.
- [128] W. Yu, H. Zhou, B.Q. Li, S. Ding, 3D printing of carbon nanotubes-based microsupercapacitors, ACS Appl. Mater. Interfaces 9 (5) (2017) 4597–4604, https://doi.org/10.1021/acsami.6b13904.
- [129] G. Sun, J. An, C.K. Chua, H. Pang, J. Zhang, P. Chen, Layer-by-layer printing of laminated graphene-based interdigitated microelectrodes for flexible planar micro-supercapacitors, Electrochem. Commun. 51 (2015) 33–36, https://doi.org/ 10.1016/j.elecom.2014.11.023.
- [130] C.M. Larson, J.J. Choi, P.A. Gallardo, S.W. Henderson, M.D. Niemack, G. Rajagopalan, R.F. Shepherd, Direct ink writing of silicon carbide for microwave optics, Adv. Eng. Mater. 18 (1) (2016) 39–45, https://doi.org/ 10.1002/adem.201500298.
- [131] S.T. Parker, P. Domachuk, J. Amsden, J. Bressner, J.A. Lewis, D.L. Kaplan, F. G. Omenetto, Biocompatible silk printed optical waveguides, Adv. Mater. 21 (23) (2009) 2411–2415.
- [132] F. Tricot, C. Venet, D. Beneventi, D. Curtil, D. Chaussy, T. Vuong, J. Broquin, N. Reverdy-Bruas, Fabrication of 3D conductive circuits: print quality evaluation of a direct ink writing process, RSC Adv. 8 (46) (2018) 26036–26046.
- [133] M. Wei, F. Zhang, W. Wang, P. Alexandridis, C. Zhou, G. Wu, 3D direct writing fabrication of electrodes for electrochemical storage devices, J. Power Sources 354 (2017) 134–147, https://doi.org/10.1016/j.jpowsour.2017.04.042.
- [134] Q. Fu, E. Saiz, A.P. Tomsia, Direct ink writing of highly porous and strong glass scaffolds for load-bearing bone defects repair and regeneration, Acta Biomater. 7 (10) (2011) 3547–3554.
- [135] J.L. Simon, S. Michna, J.A. Lewis, E.D. Rekow, V.P. Thompson, J.E. Smay, A. Yampolsky, J.R. Parsons, J.L. Ricci, In vivo bone response to 3D periodic hydroxyapatite scaffolds assembled by direct ink writing, J. Biomed. Mater. Res. Part A Off. J. Soc. Biomater. Jpn. Soc. Biomater. Aust. Soc. Biomater. Korean Soc. Biomater. 83 (3) (2007) 747–758.
- [136] Y. Chen, P. Han, L.-J. Vandi, A. Dehghan-Manshadi, J. Humphry, D. Kent, I. Stefani, P. Lee, M. Heitzmann, J. Cooper-White, A biocompatible thermoset polymer binder for direct ink writing of porous titanium scaffolds for bone tissue engineering, Mater. Sci. Eng. C 95 (2019) 160–165, https://doi.org/10.1016/j. msec.2018.10.033.
- 137 N. Sears, P. Dhavalikar, M. Whitely, E. Cosgriff-Hernandez, Fabrication of biomimetic bone grafts with multi-material 3D printing, Biofabrication 9 (2) (2017), 025020, https://doi.org/10.1088/1758-5090/aa7077.
- [138] D. Liu, P. Jiang, X. Li, J. Liu, L. Zhou, X. Wang, F. Zhou, 3D printing of metalorganic frameworks decorated hierarchical porous ceramics for high-efficiency catalytic degradation, Chem. Eng. J. 397 (2020), 125392, https://doi.org/ 10.1016/j.cej.2020.125392.
- [139] T. Ludwig, J. von Seckendorff, C. Troll, R. Fischer, M. Tonigold, B. Rieger, O. Hinrichsen, Additive manufacturing of Al2O3–based carriers for heterogeneous catalysis, Chem. Ing. Tech. 90 (5) (2018) 703–707.

- [140] S. Chandrasekaran, B. Yao, T. Liu, W. Xiao, Y. Song, F. Qian, C. Zhu, E.B. Duoss, C. M. Spadaccini, Y. Li, Direct ink writing of organic and carbon aerogels, Mater. Horiz. 5 (6) (2018) 1166–1175, https://doi.org/10.1039/c8mh00603b.
- [141] V.C.-F. Li, C.K. Dunn, Z. Zhang, Y. Deng, H.J. Qi, Direct ink write (DIW) 3D printed cellulose nanocrystal aerogel structures, Sci. Rep. 7 (1) (2017) 1–8, https://doi.org/10.1038/s41598-017-07771-y.
- [142] H. Maleki, S. Montes, N. Hayati-Roodbari, F. Putz, N. Huesing, Compressible, thermally insulating, and fire retardant aerogels through self-assembling silk fibroin biopolymers inside a silica structure—an approach towards 3D printing of aerogels, ACS Appl. Mater. Interfaces 10 (26) (2018) 22718–22730, https://doi.org/10.1021/acsami.8b05856.
- [143] M.R. Sommer, M. Schaffner, D. Carnelli, A.R. Studart, 3D printing of hierarchical silk fibroin structures, ACS Appl. Mater. Interfaces 8 (50) (2016) 34677–34685, https://doi.org/10.1021/acsami.6b11440.
- 144 T. Zhang, R.A. Sanguramath, S. Israel, M.S. Silverstein, Emulsion templating: porous polymers and beyond, Macromolecules 52 (15) (2019) 5445–5479, https://doi.org/10.1021/acs.macromol.8b02576.
- [145] C.W. Visser, D.N. Amato, J. Mueller, J.A. Lewis, Architected polymer foams via direct bubble writing, Adv. Mater. 31 (46) (2019), 1904668, https://doi.org/ 10.1002/adma.201904668.
- [146] L. Ruiz-Cantu, A. Gleadall, C. Faris, J. Segal, K. Shakesheff, J. Yang, Multi-material 3D bioprinting of porous constructs for cartilage regeneration, Mater. Sci. Eng. C 109 (2020), 110578, https://doi.org/10.1016/j.msec.2019.110578.
- [147] A. Safonov, E. Maltsev, S. Chugunov, A. Tikhonov, S. Konev, S. Evlashin, D. Popov, A. Pasko, I. Akhatov, Design and fabrication of complex-shaped ceramic bone implants via 3d printing based on laser stereolithography, Appl. Sci. 10 (20) (2020) 7138.
- [148] Q. Ge, Z. Li, Z. Wang, K. Kowsari, W. Zhang, X. He, J. Zhou, N.X. Fang, Projection micro stereolithography based 3D printing and its applications, Int. J. Extrem. Manuf. 2 (2) (2020), 022004.
- [149] R. He, G. Ding, K. Zhang, Y. Li, D. Fang, Fabrication of SiC ceramic architectures using stereolithography combined with precursor infiltration and pyrolysis, Ceram. Int. 45 (11) (2019) 14006–14014, https://doi.org/10.1016/j. ceramint.2019.04.100.
- 150 R. Gauvin, Y.-C. Chen, J.W. Lee, P. Soman, P. Zorlutuna, J.W. Nichol, H. Bae, S. Chen, A. Khademhosseini, Microfabrication of complex porous tissue engineering scaffolds using 3D projection stereolithography, Biomaterials 33 (15) (2012) 3824–3834, https://doi.org/10.1016/j.biomaterials.2012.01.048.
- [151] C. Zhou, Y. Chen, Z. Yang, B. Khoshnevis, Digital material fabrication using maskimage-projection-based stereolithography, Rapid Prototyp, J. 19 (2013) 153–165.
- [152] N. Anandakrishnan, H. Ye, Z. Guo, Z. Chen, K.I. Mentkowski, J.K. Lang, N. Rajabian, S.T. Andreadis, Z. Ma, J.A. Spernyak, Fast stereolithography printing of large-scale biocompatible hydrogel models, Adv. Healthc. Mater. 10 (10) (2021), 2002103, https://doi.org/10.1002/adhm.202002103.
- [153] R.M. Hensleigh, H. Cui, J.S. Oakdale, C.Y. Jianchao, P.G. Campbell, E.B. Duoss, C. M. Spadaccini, X. Zheng, M.A. Worsley, Additive manufacturing of complex micro-architected graphene aerogels, Mater. Horiz. 5 (6) (2018) 1035–1041.
- [154] E. Shukrun Farrell, Y. Schilt, M.Y. Moshkovitz, Y. Levi-Kalisman, U. Raviv, S. Magdassi, 3D Printing of ordered mesoporous silica complex structures, Nano Lett. 20 (9) (2020) 6598–6605.
- [155] R. Fu, B. Zheng, J. Liu, M.S. Dresselhaus, G. Dresselhaus, J.H. Satcher Jr., T. F. Baumann, The fabrication and characterization of carbon aerogels by gelation and supercritical drying in isopropanol, Adv. Funct. Mater. 13 (7) (2003) 558–562.
- 156 C. Ma, R. Wang, H. Tetik, S. Gao, M. Wu, Z. Tang, D. Lin, D. Ding, W. Wu, Hybrid nanomanufacturing of mixed-dimensional manganese oxide/graphene aerogel macroporous hierarchy for ultralight efficient supercapacitor electrodes in self-powered ubiquitous nanosystems, Nano Energy 66 (2019), 104124.
- [157] J. Ding, K. Shen, Z. Du, B. Li, S. Yang, 3D-printed hierarchical porous frameworks for sodium storage, ACS Appl. Mater. Interfaces 9 (48) (2017) 41871–41877, https://doi.org/10.1021/acsami.7b12892.
- [158] Y. Jiang, Z. Xu, T. Huang, Y. Liu, F. Guo, J. Xi, W. Gao, C. Gao, Direct 3D printing of ultralight graphene oxide aerogel microlattices, Adv. Funct. Mater. 28 (16) (2018), 1707024, https://doi.org/10.1002/adfm.201707024.
- [159] C. Simón-Herrero, S. Caminero-Huertas, A. Romero, J.L. Valverde, L. Sánchez-Silva, Effects of freeze-drying conditions on aerogel properties, J. Mater. Sci. 51 (19) (2016) 8977–8985, https://doi.org/10.1007/s10853-016-0148-5.
- [160] V.P. Oikonomopoulou, M.K. Krokida, V.T. Karathanos, The influence of freeze drying conditions on microstructural changes of food products, Procedia Food Sci. 1 (2011) 647–654.
- [161] T. Fukasawa, M. Ando, T. Ohji, S. Kanzaki, Synthesis of porous ceramics with complex pore structure by freeze-dry processing, J. Am. Ceram. Soc. 84 (1) (2001) 230–232, https://doi.org/10.1111/j.1151-2916.2001.tb00638.x.
- [162] F. Putz, S. Scherer, M. Ober, R. Morak, O. Paris, N. Hüsing, 3D printing of hierarchical porous silica and α-quartz, Adv. Mater. Technol. 3 (7) (2018), 1800060, https://doi.org/10.1002/admt.201800060.
- [163] H. Françon, Z. Wang, A. Marais, K. Mystek, A. Piper, H. Granberg, A. Malti, P. Gatenholm, P.A. Larsson, L. Wågberg, Ambient-dried, 3D-Printable and electrically conducting cellulose nanofiber aerogels by inclusion of functional polymers, Adv. Funct. Mater. 30 (12) (2020), 1909383, https://doi.org/10.1002/ adfm.201909383.
- [164] A. Jakus, N. Geisendorfer, P. Lewis, R. Shah, 3D-printing porosity: a new approach to creating elevated porosity materials and structures, Acta Biomater. 72 (2018) 94–109, https://doi.org/10.1016/j.actbio.2018.03.039.

- [165] H. Bai, Y. Chen, B. Delattre, A.P. Tomsia, R.O. Ritchie, Bioinspired large-scale aligned porous materials assembled with dual temperature gradients, Sci. Adv. 1 (11) (2015), e1500849, https://doi.org/10.1126/sciadv.1500849.
- 166 P. Niksiar, F.Y. Su, M.B. Frank, T.A. Ogden, S.E. Naleway, M.A. Meyers, J. McKittrick, M.M. Porter, External field assisted freeze casting, Ceramics 2 (1) (2019) 208–234.
- [167] G. Shao, D.A. Hanaor, X. Shen, A. Gurlo, Freeze casting: from low-dimensional building blocks to aligned porous structures—a review of novel materials, methods, and applications, Adv. Mater. 32 (17) (2020), 1907176, https://doi. org/10.1002/adma.201907176.
- [168] I. Nelson, S.E. Naleway, Intrinsic and extrinsic control of freeze casting, J. Mater. Res. Technol. 8 (2) (2019) 2372–2385, https://doi.org/10.1016/j. imrt 2018 11 011
- [169] H. Tetik, D. Feng, S.W. Oxandale, G. Yang, K. Zhao, K. Feist, N. Shah, Y. Liao, Z. C. Leseman, D. Lin, Bioinspired manufacturing of aerogels with precisely manipulated surface microstructure through controlled local temperature gradients, ACS Appl. Mater. Interfaces 13 (1) (2021) 924–931, https://doi.org/10.1021/acsami.0c19087.
- [170] I. Gibson, M.F. Ashby, The mechanics of three-dimensional cellular materials, Proc. R. Soc. Lond. A Math. Phys. Sci. 382 (1782) (1982) 43–59.
- [171] S. Tarafder, V.K. Balla, N.M. Davies, A. Bandyopadhyay, S. Bose, Microwave-sintered 3D printed tricalcium phosphate scaffolds for bone tissue engineering, J. Tissue Eng. Regen. Med. 7 (8) (2013) 631–641.
- [172] R. Brezny, D.J. Green, The effect of cell size on the mechanical behavior of cellular materials, Acta Metall. Et. Mater. 38 (12) (1990) 2517–2526, https://doi. org/10.1016/0956-7151(90)90263-G.
- [173] N. Kleger, M. Cihova, K. Masania, A.R. Studart, J.F. Löffler, 3D printing of salt as a template for magnesium with structured porosity, Adv. Mater. 31 (37) (2019), 1903783, https://doi.org/10.1002/adma.201903783.
- [174] S.D. Lacey, D.J. Kirsch, Y. Li, J.T. Morgenstern, B.C. Zarket, Y. Yao, J. Dai, L. Q. Garcia, B. Liu, T. Gao, Extrusion-based 3D printing of hierarchically porous advanced battery electrodes, Adv. Mater. 30 (12) (2018), 1705651, https://doi.org/10.1002/adma.201705651.
- [175] Z. Wang, X. Guan, H. Huang, H. Wang, W. Lin, Z. Peng, Full 3D printing of stretchable piezoresistive sensor with hierarchical porosity and multimodulus architecture, Adv. Funct. Mater. 29 (11) (2019), 1807569, https://doi.org/ 10.1002/adfm.201807569.
- 176 B. Grigoryan, S.J. Paulsen, D.C. Corbett, D.W. Sazer, C.L. Fortin, A.J. Zaita, P. T. Greenfield, N.J. Calafat, J.P. Gounley, A.H. Ta, Multivascular networks and functional intravascular topologies within biocompatible hydrogels, Science 364 (6439) (2019) 458–464, https://doi.org/10.1126/science.aav9750.
- [177] S. Chowdhury, R. Balasubramanian, Recent advances in the use of graphenefamily nanoadsorbents for removal of toxic pollutants from wastewater, Adv. Colloid Interface Sci. 204 (2014) 35–56.
- [178] D. Zhang, J. Xiao, Q. Guo, J. Yang, 3D-printed highly porous and reusable chitosan monoliths for Cu (II) removal, J. Mater. Sci. 54 (8) (2019) 6728–6741.
- [179] K. Fu, Y. Wang, C. Yan, Y. Yao, Y. Chen, J. Dai, S. Lacey, Y. Wang, J. Wan, T. Li, Graphene oxide-based electrode inks for 3D-printed lithium-ion batteries, Adv. Mater. 28 (13) (2016) 2587–2594, https://doi.org/10.1002/adma.201505391.
- [180] A. Iakunkov, V. Skrypnychuk, A. Nordenström, E.A. Shilayeva, M. Korobov, M. Prodana, M. Enachescu, S.H. Larsson, A.V. Talyzin, Activated graphene as a material for supercapacitor electrodes: effects of surface area, pore size distribution and hydrophilicity, Phys. Chem. Chem. Phys. 21 (32) (2019) 17901–17912, https://doi.org/10.1039/C9CP03327K.
- [181] P. Chen, H. Chen, J. Qiu, C. Zhou, Inkjet printing of single-walled carbon nanotube/RuO 2 nanowire supercapacitors on cloth fabrics and flexible substrates, Nano Res. 3 (8) (2010) 594–603, https://doi.org/10.1007/s12274-010-0020-x.
- [182] H. Jung, C. Ve Cheah, N. Jeong, J. Lee, Direct printing and reduction of graphite oxide for flexible supercapacitors, Appl. Phys. Lett. 105 (5) (2014), 053902.
- [183] J. Jiang, H. Oguzlu, F. Jiang, 3D printing of lightweight, super-strong yet flexible all-cellulose structure, Chem. Eng. J. 405 (2021), 126668, https://doi.org/ 10.1016/j.cej.2020.126668.
- 184 R. Ajdary, S. Huan, N. Zanjanizadeh Ezazi, W. Xiang, R. Grande, Hl.A. Santos, O. J. Rojas, Acetylated nanocellulose for single-component bioinks and cell proliferation on 3D-printed scaffolds, Biomacromolecules 20 (7) (2019) 2770–2778, https://doi.org/10.1021/acs.biomac.9b00527.
- [185] E. Espinosa, D. Filgueira, A. Rodríguez, G. Chinga-Carrasco, Nanocellulose-based inks—effect of alginate content on the water absorption of 3d printed constructs, Bioengineering 6 (3) (2019) 65, https://doi.org/10.3390/ bioengineering6030065.
- [186] J.V. John, A. McCarthy, H. Wang, Z. Luo, H. Li, Z. Wang, F. Cheng, Y.S. Zhang, J. Xie, Freeze-casting with 3D-printed templates creates anisotropic microchannels and patterned macrochannels within biomimetic nanofiber aerogels for rapid cellular infiltration, Adv. Healthc. Mater. 10 (2021), 2100238, https://doi.org/10.1002/adhm.202100238.
- [187] H.-W. Kang, S.J. Lee, I.K. Ko, C. Kengla, J.J. Yoo, A. Atala, A 3D bioprinting system to produce human-scale tissue constructs with structural integrity, Nat. Biotechnol. 34 (3) (2016) 312–319, https://doi.org/10.1038/nbt.3413.
- [188] R. Trombetta, J.A. Inzana, E.M. Schwarz, S.L. Kates, H.A. Awad, 3D printing of calcium phosphate ceramics for bone tissue engineering and drug delivery, Ann. Biomed. Eng. 45 (1) (2017) 23–44.
- 189 C. Polley, T. Distler, R. Detsch, H. Lund, A. Springer, A.R. Boccaccini, H. Seitz, 3D printing of piezoelectric barium titanate-hydroxyapatite scaffolds with interconnected porosity for bone tissue engineering, Materials 13 (7) (2020) 1773, https://doi.org/10.3390/ma13071773.

- [190] Y. Ji, Y. Ma, Y. Ma, J. Asenbauer, S. Passerini, C. Streb, Water decontamination by polyoxometalate-functionalized 3D-printed hierarchical porous devices, Chem. Commun. 54 (24) (2018) 3018–3021, https://doi.org/10.1039/C8CC00821C.
- [191] X. Xu, S. Xiao, H.J. Willy, T. Xiong, R. Borayek, W. Chen, D. Zhang, J. Ding, 3D-printed grids with polymeric photocatalytic system as flexible air filter, Appl. Catal. B Environ. 262 (2020), 118307, https://doi.org/10.1016/j.apcatb.2019.118307
- [192] O. Doutres, N. Atalla, K. Dong, Effect of the microstructure closed pore content on the acoustic behavior of polyurethane foams, J. Appl. Phys. 110 (6) (2011), 064901, https://doi.org/10.1063/1.3631021.
- [193] H. Tetik, Y. Wang, X. Sun, D. Cao, N. Shah, H. Zhu, F. Qian, D. Lin, Additive manufacturing of 3D aerogels and porous scaffolds: a review, Adv. Funct. Mater. (2021), 2103410, https://doi.org/10.1002/adfm.202103410.
- [194] T. Gao, Z. Zhou, J. Yu, J. Zhao, G. Wang, D. Cao, B. Ding, Y. Li, 3D printing of tunable energy storage devices with both high areal and volumetric energy densities, Adv. Energy Mater. 9 (8) (2019), 1802578, https://doi.org/10.1002/ aenm.20180257.
- 195 X. Tian, K. Zhou, 3D printing of cellular materials for advanced electrochemical energy storage and conversion, Nanoscale 12 (14) (2020) 7416–7432, https://doi. org/10.1039/D0NR00291G.

- [196] S. Lawson, X. Li, H. Thakkar, A.A. Rownaghi, F. Rezaei, Recent advances in 3D printing of structured materials for adsorption and catalysis applications, Chem. Rev. 121 (10) (2021) 6246–6291, https://doi.org/10.1021/acs.abspaces.1200600
- [197] N.D. Sanandiya, Y. Vijay, M. Dimopoulou, S. Dritsas, J.G. Fernandez, Large-scale additive manufacturing with bioinspired cellulosic materials, Sci. Rep. 8 (1) (2018) 1–8, https://doi.org/10.1038/s41598-018-26985-2.
- [198] A. Kazemian, X. Yuan, E. Cochran, B. Khoshnevis, Cementitious materials for construction-scale 3D printing: laboratory testing of fresh printing mixture, Constr. Build. Mater. 145 (2017) 639–647, https://doi.org/10.1016/j. conbuildmat.2017.04.015.
- [199] X. Zong, H. Hu, G. Ouyang, J. Wang, R. Shi, L. Zhang, Q. Zeng, C. Zhu, S. Chen, C. Cheng, Black phosphorus-based van der Waals heterostructures for mid-infrared light-emission applications, Light. Sci. Appl. 9 (1) (2020) 1–8, https://doi.org/10.1038/s41377-020-00356-x.
- [200] J. Han, K. Xie, Z. Du, W. Zou, C. Zhang, β-Cyclodextrin functionalized polystyrene porous monoliths for separating phenol from wastewater, Carbohydr. Polym. 120 (2015) 85–91.